Targeting ALC1 can safely expand the therapeutic utility of PARP inhibitors across high-grade serous ovarian cancers

Lindsey N. Aubuchon[*1,2], Deanna H. Wong[*1,3,4], Natasha M. Ramakrishnan[1], Rohan Reddy[1], Amanda Compadre[3,4], Elena Lomonosova[3,4], Kathleen E. Jackson[1], Danielle Kemper[1], Vrutti Mehta[1], Kellen Zoberi[1], Dineo Khabele[3,4], Elizabeth L. Christie[5], Mary M. Mullen[3,4], Priyanka Verma[#1,4]

1. Division of Oncology, Department of Medicine, Siteman Cancer Center, Washington University School of Medicine, St. Louis, MO, 63110, USA

2. Cancer Biology Graduate Program, Washington University School of Medicine, St. Louis, MO, 63110, USA

3. Division of Gynecologic Oncology, Department of Obstetrics and Gynecology, Siteman Cancer Center, Washington University, St. Louis, Missouri, USA.

4. Center for Reproductive Health Sciences, Department of Obstetrics and Gynecology, Siteman Cancer Center, Washington University School of Medicine, 4911 Barnes Jewish Hospital Plaza, St. Louis, Missouri 63110, USA

5. Sir Peter MacCallum Department of Oncology, The University of Melbourne, Parkville, Victoria, Australia.

* Co-first authors

Corresponding author; vermap@wustl.edu

Abstract

- Poly (ADP-ribose) polymerase inhibitors (PARPi) are approved for homologous recombination-deficient (HRD) high-grade serous ovarian cancers (HGSOCs), but their long-term effectiveness is limited by the emergence of resistance and hematological toxicity. Approximately 50% of HGSOCs are homologous recombination-proficient (HRP), and within this group, about 20% harbor *CCNE1* amplification (cyclin E1-high). PARPi are especially ineffective in HRP tumors and in *CCNE1*-high HGSOCs, which represent a major unmet clinical need. Loss of a chromatin remodeling enzyme, Amplified in Liver Cancer 1, ALC1, has been shown to enhance PARPi sensitivity. However, the clinical contexts in which ALC1 targeting will be clinically meaningful remains unclear. Here we demonstrate that ALC1 loss can enhance PARPi sensitivity across HRD and cyclin E1-high serous ovarian cancer lines, xenografts and patient-derived cells. ALC1 depletion can overcome several clinically relevant mechanisms of PARPi resistance, though its impact is limited in tumors with complete restoration of HR. Lower ALC1 expression correlates with longer progression-free survival and extended PARPi response. Importantly, ALC1 loss has minimal effects in *BRCA*-wild-type or *BRCA*-heterozygous non-cancerous fallopian tube cells, suggesting therapeutic safety. Increased PARPi sensitivity following ALC1 loss can be accurately predicted by endogenous single-stranded DNA levels, identifying a functional biomarker. Together, our studies define the clinical contexts in which the therapeutic utility of PARPi can be expanded by targeting ALC1, whose inhibitors are currently under evaluation in Phase I clinical trials.

Introduction

High-grade serous ovarian cancer (HGSOCs) is the deadliest gynecologic malignancy in the United States, with approximately 13,000 women dying from the disease each year[1]. Whole genome sequencing of HGSOCs revealed that while approximately 50% of these tumors have evidence of homologous recombination (HR) deficiency, another 20% are HR-proficient and associated with amplification of an oncogene *CCNE1* (cyclinE1-high)[2]. The treatment regimen for HR-deficient (HRD) serous ovarian cancers includes Poly (ADP-ribose) polymerase inhibitors (PARPi), a frontline and maintenance therapy for platinum-sensitive tumors. However, major challenges associated with clinical success of PARPi include inevitable emergence of resistance and development of hematological disorders[3,4]. Cyclin E1-high HGSOCs, on the other hand, display resistance to both platinum and PARPi-based therapies[5]. Currently, there are no FDA-approved approaches to reduce effective PARPi dosage for alleviating toxicity, or to make this targeted therapy effective in the context of cyclin E1-high serous ovarian cancers.

The potency of PARPi in killing cells emanates from their ability to trap PARP1 and 2 enzymes on the chromatin[6,7]. Trapped PARP1 and 2 enzymes impede fork progression and result in replication-coupled gaps and breaks, which increase the reliance on HR proteins for repair and survival. Hence, trapping potency of various PARPi directly correlates with cell cytotoxicity. In cells, talazoparib is the most potent PARP1/2 trapper and induces the most cytotoxicity, followed by niraparib. Olaparib and rucaparib share similar PARP1/2 trapping potency, albeit weaker than talazoparib and niraparib. Compared to these PARPi,

veliparib is a weaker PARP1/2 trapper and hence it displays greatly reduced potency in cell killing[6,7]. In concordance with higher trapping leading to more cytotoxicity, incidences of anemia and cytopenia are more common with talazoparib and niraparib. In contrast, veliparib, despite its reduced toxicity and lack of susceptibility to multi-drug efflux pumps, has not shown meaningful efficacy in several clinical trials[8]. Currently, niraparib, olaparib and rucaparib are approved as frontline and maintenance therapies for platinum-sensitive HGSOCs. To address the limitations of PARPi, there are ongoing efforts to design combinatorial strategies. However, it is unclear if different PARPi will display similar potency in killing cancer cells when used in combination with other agents. Moreover, how the unique properties of talazoparib and veliparib can be exploited to develop effective combinatorial strategies for ovarian cancer regimen remains elusive.

We previously pursued a CRISPR screen to identify factors that can enhance PARPi sensitivity in UWB1.289, a *BRCA1*-mutant HGSOC cancer cell line[9,10]. One of the top candidates that emerged from the screen was a nucleosome sliding enzyme called Amplified in Liver Cancer 1 (ALC1) (**Fig.1a**) [9,10]. More recently, we demonstrated that ALC1 mediated chromatin remodeling is specifically required for the repair of chromatin-buried abasic sites[11], an intermediate formed during base excision repair or generated by the spontaneous loss of a nitrogen base from single-strand DNA[12]. ALC1 is dispensable for responses to many other genotoxins. Furthermore, ALC1 knockout mice are viable and do not display a compromise in fitness or cancer predisposition[10]. These unique features have recently propelled the entry of ALC1 inhibitors into a Phase I clinical trial (NCT06525298). However, the contexts in which ALC1 targeting will be most fruitful to enhance PARPi sensitivity remain unclear. Moreover, a functional biomarker platform to predict PARPi efficacy after ALC1 targeting remains to be defined.

Here, we report that reduced ALC1 protein levels correlate with better progression-free survival and longer time on PARPi as a maintenance therapy in individuals with HRD-ovarian cancers. We demonstrate that ALC1 loss can significantly enhance sensitivity to various PARPi across multiple HGSOC contexts, which include platinum-sensitive *BRCA1/2*-mutant, platinum-resistant *BRCA1/2*-mutant, as well as cyclin E1-high cancer cell lines. We validated PARPi sensitivity of ALC1-deficient Cyclin E1-HGSOCs cells in a xenograft model. We also demonstrate that ALC1 loss has minimal to no impact on genome stability and PARPi response in *BRCA*-WT and *BRCA*-heterozygous non-cancerous fallopian tube cell lines, highlighting the safety associated with ALC1 targeting. Finally, we identify that levels of single-stranded DNA as quantified by chromatin-bound replication protein A (RPA) can be used as a reliable and quantitative functional biomarker to predict enhancement in PARPi sensitivity upon ALC1 loss. Together, this study suggests that targeting ALC1 can be a safe and clinically actionable approach to treat a wide spectrum of HGSOCs using PARPi.

Results

High levels of ALC1 are present in primary ovarian tumors and is associated with poor prognosis

We examined publicly available The Cancer Genome Atlas (TCGA) data for 602 HGSOCs deposited in cBioPortal to assess for genomic alterations in ALC1[13]. Approximately 7% of cases were associated with amplification in the *ALC1* (**Fig. 1b**), suggesting an increased expression of this gene in ovarian cancer. In concordance, assessment of ALC1 protein levels using immunohistochemistry analysis of tissue-microarray revealed a significantly higher protein expression in primary serous ovarian tumors (n=142) as compared to benign tissue samples (n=51) (**Fig. 1c**). Higher levels of ALC1 in tumors therefore provide the

opportunity to target this protein for therapeutic utility. We next used the Kaplan-Meier Plotter, which integrates 1816 ovarian cancer samples from 17 independent databases, including TCGA, to examine the impact of ALC1 expression on progression-free and overall survival. All four expression probe sets showed a significant association between higher ALC1 and poor progression-free survival (**Fig. 1d**). Additionally, two of the four probes showed a significant correlation between high ALC1 level and poor overall survival (**Fig. 1e**)[14]. We next examined previously published proteomics data from HRD HGSOC tumors to assess the correlation between ALC1 protein levels and estimated time individuals were on PARPi treatment (**Table 1**)[15]. We observe that low ALC1 levels trend with longer treatment with PARPi (**Fig. 1f)**. Together, these data establish the clinical rationale for targeting ALC1 in HGSOCs. We next set out to identify ovarian cancer contexts in which ALC1 targeting can be clinically meaningful.

ALC1 loss enhances sensitivity to various PARPi but not cisplatin across multiple *BRCA1/2*- mutant HGSOC cell lines

We have previously shown that ALC1 loss enhances olaparib sensitivity of UWB1.289, a *BRCA1*-mutant ovarian cancer cell line[9]. We first examined whether this sensitivity could be extended to other PARPi. To do so, we depleted ALC1 using a previously established SaCas9-sgRNA strategy[9] and assessed sensitivity to olaparib, rucaparib, niraparib and veliparib. Consistent with our previous findings, ALC1 depletion significantly enhanced sensitivity of UWB1.289 cells to olaparib. In addition, *ALC1*-deficient UWB1.289 cells were more sensitive to rucaparib, niraparib and veliparib as compared to their parental counterparts. A similar drug sensitivity profile upon ALC1 loss was also observed in JHOS4, another *BRCA1*-mutant HGSOC cell line. Together, these findings suggest that targeting ALC1 can enhance the sensitivity of *BRCA1*-mutant HGSOC to various PARPi (**Fig. 2a, b)**.

We next examined the impact of ALC1 depletion on PARPi responses in the *BRCA2*-mutant HGSOC cell line, OVSAHO. ALC1 loss in OVSAHO cells enhanced sensitivity to olaparib, rucaparib and niraparib. Minimal enhancement in veliparib sensitivity was observed in *ALC1*-deficient OVSAHO cells (**Fig. 2a, b**). In both *BRCA1/2*-mutant settings, ALC1 loss showed stronger sensitization to rucaparib and olaparib, suggesting that the intermediate trapping potential of these PARPi may make them more favorable for combinatorial therapies[6].

We also tested the impact of ALC1 loss on sensitivity to cisplatin, a platinum-based therapy. Notably, ALC1 loss did not enhance sensitivity to cisplatin in either *BRCA1* or *BRCA2*-deficient cells (**Fig. 2a, b**). Cisplatin-induced double-strand break (DSB) repair in HRD settings can be performed by microhomology-mediated end joining (MMEJ)[16,17]. Our data showing the dispensability of ALC1 in cisplatin response, both in *BRCA1* and *2*-mutant settings, suggests that this chromatin remodeler likely does not contribute to MMEJ. To experimentally validate that ALC1 is dispensable for MMEJ, we used a published reporter assay[18]. The assay entails I-SceI nuclease-mediated generation of a DSB at a locus flanked by microhomology. Repair of the I-SceI-induced break by MMEJ results in annealing of the microhomology arm to generate an open reading frame for the expression of mCherry protein (**Fig. 2c**). Consistent with dispensability of ALC1 for MMEJ, loss of ALC1 did not have a significant impact on mCherry signal in the MMEJ reporter assay. In contrast, depletion of Polymerase Theta, a bona fide component of MMEJ, substantially reduced mCherry signal (**Fig. 2c**). ALC1 dispensability for MMEJ highlights its unique mechanism of action compared to Polymerase Theta inhibitors, which are currently in clinical trials for treatment of multiple forms of HRD-ovarian cancers[19].

ALC1 loss sensitizes HR-proficient cyclin E1-high cells and xenograft models to PARPi

Approximately 20% of HGSOCs are associated with amplification of *CCNE1*[2]. Individuals with cyclin E1-high ovarian cancers display poor prognosis and resistance to platinum- and PARPi-based treatments because of their proficiency in HR[20,21]. Notably, CCNE1 amplification and HR deficiency are almost entirely mutually exclusive, as cyclin E1–high tumors retain intact HR function and rarely harbor BRCA1/2 mutations or other HRD-associated genomic alterations. We first examined whether HR-proficiency was retained in cell line models of cyclin E1-high HGSOCs. To test this, we used two cell lines, OVCAR3 and OVCAR4, which exhibit amplification of the cyclin E1-encoding gene, *CCNE1*, as well as OVCAR8, which shows a gain in *CCNE1* copy number[22]. These cell lines displayed proficiency in Rad51 foci formation, establishing their HR-proficient status (**Supp. Fig. 2**). Cyclin E1 high cells are established to have increased levels of replication stress, which results in the accumulation of single-strand DNA[23,24]. Single-stranded DNA can spontaneously undergo loss of nitrogen bases resulting in formation of abasic sites, lesions that underlie PARPi hypersensitivity in ALC1-deficient cells[11,32]. We therefore hypothesized that increased single-stranded DNA in cyclin E1-high cancer cells may render them sensitive to PARPi treatment upon ALC1 depletion. Consistent with this proposition, we indeed observed that ALC1 depletion profoundly enhanced olaparib and rucaparib sensitivity in OVCAR3, OVCAR4 and OVCAR8 cells (**Fig. 3a, b**). In line with our prior observations, the impact of ALC1 loss on niraparib sensitivity was modest in cyclin E1-high cells as well. Our observations therefore highlight that targeting ALC1 can be an effective therapeutic approach to sensitize chemo resistant cyclin E1-high ovarian cancers to PARPi. Additionally, ALC1 loss did not impact sensitivity to cisplatin, supporting its dispensability for HR repair.

We next extended our findings in cyclin E1-high cells to xenograft models. To do so, we utilized OVCAR8 cells, since they have been established to form ovarian tumors in mice[25]. OVCAR8 cells were engineered with sgRNAs targeting either *ALC1* or the safe locus *AAVS1* as a negative control. After puromycin treatment to select for cells with sgRNAs, the cells were intraperitoneally injected into nude mice. At 14 days, two mice from each of the sg*AAVS1* and sg*ALC1* groups were sacrificed and analyzed to ensure development of ovarian tumor nodules. Starting on the 14th day after tumor injection, 10 mice from each of the sg*AAVS1* and sg*ALC1* groups were administered 50mg/kg of olaparib via oral gavage every third day, while another group was administered vehicle control. On the 35th day after initiation of PARPi treatment, mice were sacrificed to measure tumor weight and nodules (**Fig. 3c**). Consistent with the chemoresistance of OVCAR8, olaparib treatment in sg*AAVS1* group did not have an impact on tumor growth. In contrast, olaparib-treated sg*ALC1* cells showed significantly reduced tumor growth and tumor nodules (**Fig. 4d**). Together, our cell line and xenograft studies collectively suggest that targeting ALC1 can expand the utility of PARPi for the treatment of cyclin E1-high serous ovarian cancers, which currently have limited to no chemotherapeutic options.

ALC1 loss restores PARPi sensitivity across various clinically relevant models of chemo-resistant ovarian cancers

Given that ALC1 loss can significantly enhance PARPi sensitivity in HR-proficient cyclin E1-high ovarian cancer cells, we next examined if this impact can be extended in chemoresistance models of *BRCA*-mutant ovarian cancers. *BRCA1*-mutant ovarian cancer cells eventually develop resistance when exposed to PARPi for a prolonged period. Mechanistically, this is due to rewiring of ATR signaling, which enables Rad51 loading at DNA breaks and reversed forks independent of BRCA1 protein[26]. This has been the key rationale for multiple ongoing clinical trials for ovarian cancers involving a combination of ATR inhibitor (ATRi)

and PARPi. While the results of combining ATRi and PARPi have been promising across multiple clinical trials, the adverse side effects of cytopenia and severe anemia have limited its clinical translation[27]. We examined whether ALC1 depletion might counteract PARPi resistance arising from the ATR-dependent repair compensating for compromised BRCA1 activity. To do so, we procured two UWB1.289 cell lines, SYr12 and SYr14, that have acquired PARPi resistance by increasing reliance on ATR-mediated Rad51 loading at DNA double-strand breaks and reversed forks[26] (**Supp. Fig. 2a**). Notably, ALC1 loss imparts sensitivity to olaparib and rucaparib in both SYr12 and SYr14 cell lines, highlighting that targeting ALC1 can be a viable approach to overcome PARPi resistance in *BRCA1*-mutant ovarian cancers that have bypassed the functional requirement of BRCA1 by increasing reliance on ATR activity (**Fig. 4a, b**).

Many pathogenic mutations in *BRCA1* do not abrogate the expression of the entire protein but instead result in overexpression of various hypomorphs. Overexpression of BRCA1 hypomorphs is yet another commonly reported mechanism of PARPi resistance in ovarian cancer[28–32] (**Supp. Fig. 2b,c**). To examine if ALC1 loss can restore PARPi sensitivity in ovarian cancer cells that have acquired resistance due to overexpression of hypomorphs, we procured UWB1.289 cells that are PARPi resistant due to overexpression of the del l1q isoform of BRCA1[31]. This isoform is derived by alternative splicing wherein most nucleotides in exon 11 (c.788-4096) are lost. We observe that depletion of ALC1 enhances sensitivity of UWB1.289 overexpressing del l1q BRCA1 hypomorphs to olaparib and rucaparib (**Supp. Fig. 2d**). To extend our findings to a more clinically relevant setting, we derived patient cells from a relapsed platinum-resistant tumor of an individual with *BRCA1* promoter methylation. Strikingly, depletion of ALC1 in these primary cells conferred enhanced sensitivity to olaparib, rucaparib and niraparib (**Fig. 4b**). We next explored another potential resistant model wherein *BRCA1* is exogenously overexpressed in the UWB1.289 cell line[33]. Consistent with the dispensability of ALC1 in HR, depletion of this protein in cells with BRCA1 overexpression did not enhance sensitivity to olaparib, rucaparib, niraparib or cisplatin. However, we observe that ALC1 loss can increase talazoparib sensitivity in cells overexpressing BRCA1 WT protein (**Fig. 4a, b**). Together, our studies suggest that while targeting ALC1 can be a viable approach to restore PARPi sensitivity in tumors that have partially restored HR, its therapeutic utility in HGSOCs with BRCA1 overexpression could be limited. Under the conditions of full length *BRCA1* overexpression, combining ALC1 targeting with talazoparib can be considered as a potential therapeutic option.

ALC1 loss does not impact PARPi responses or genome stability in *BRCA*-WT and heterozygous fallopian tube cells

The minimal impact of ALC1 in *BRCA*-proficient UWB1.289 cells suggested that targeting this remodeler may have minimal impact on normal healthy cells. To test this, we used a panel of cell lines derived from normal fallopian tube (FT) epithelium, the tissue where the majority of HGSOCs originate[34,35]. The FT cell line panel included hTERT-immortalized FT190, FT194 and FT282. Remarkably, ALC1 loss did not enhance sensitivity to either platinum or any PARPi including talazoparib (**Fig. 5a, b**). We next extended our studies in the context of non-cancerous *BRCA1*-heterozygous FT epithelial cells. This scenario represents normal healthy cells in individuals who are born with a pathological copy of the *BRCA1 or 2* gene and hence are heterozygous for the mutation at the organismal level[36]. To do so, we used CRISPR/Cas9 to generate two different FT282 clones with *BRCA1* heterozygous genotype. We confirmed the heterozygous status of the cell line using next-generation sequencing and western blotting (**Supp. Fig. 3**). ALC1 loss had minimal to no impact on PARPi or platinum responses in *BRCA1*-heterozygous FT282 cells (**Fig. 6a, b**) as well, reinforcing the potential safety associated with targeting this chromatin for therapeutic purposes.

To further establish that ALC1 targeting is likely to have minimal impact on normal non-cancerous cells, we assessed how loss of this remodeler impacts genome stability in *BRCA1*-WT FT282, *BRCA1*-heterozygous FT282 and *BRCA1*-mutant UWB1.289 cells. We determined levels of replication stress and replication-coupled double-strand breaks by quantifying pS33-RPA and γH2AX respectively. ALC1 loss did not enhance either pS33-RPA or γH2AX levels in *BRCA1*-WT FT282 cells. In *BRCA1*-heterozygous FT282 cells, ALC1-deficiency showed a modest 1.2-fold increase in pS33-RPA with no concomitant increase in γH2AX. The modest enhancement in pS33-RPA could be due to the inability of *BRCA*-heterozygous cells to resolve replication stress[37,38], which can be generated upon ALC1 loss. Unresolved replication stress eventually results in DNA double-strand breaks. We reason that the proficiency of *ALC1*-deficient *BRCA1*-heterozygous cells in HR repair can eventually resolve any genome instability that arises due to the modest increase in replication stress. Indeed, we do not observe an increase in double-strand breaks in ALC1-deficient *BRCA1*-heterozygous cells compared to their ALC1-proficient counterparts. Unlike in *BRCA1*-WT and *BRCA1*-heterozygous FT282 cells, ALC1 loss in *BRCA1*-mutant UWB1.289 cells resulted in a 1.4- and 1.7-fold increase in pS33-RPA or γH2AX respectively (**Fig. 6c, d**). Together, these observations strengthen the validity of ALC1 as a safe target while concomitantly hypersensitizing multiple forms of HGSOCs to PARPi.

Endogenous level of chromatin-bound RPA is a predictor of enhancement in PARPi response upon ALC1 depletion

Our data showing a selective impact of ALC1 loss on PARPi responses in cancer cells over non-cancer counterparts highlights that targeting the ALC1 remodeler likely exploits a vulnerability intrinsic to cancer cells. Our recent work has demonstrated that enhanced PARPi sensitivity upon ALC1 loss is reliant on the role of this remodeler in promoting the repair of chromatin-buried abasic sites[11]. Unfortunately, there are no tools available that are sensitive enough to quantify the levels of endogenous abasic sites in cells. Spontaneous generation of abasic sites in cells occurs in the context of single-stranded DNA[39]. We therefore reasoned that levels of single-stranded DNA, which can be quantified by chromatin-bound RPA, can predict the propensity of spontaneous abasic site formation and thereby enhanced PARPi response in ALC1-deficient cells. To test this, we quantified endogenous levels of chromatin-bound RPA in a panel of cell lines that can or cannot be sensitized to PARPi upon ALC1 depletion. We observe a strong direct correlation between endogenous levels of chromatin-bound RPA and fold enhancement in sensitivity to both olaparib (R^2:0.7427) and rucaparib (R^2:0.9372) (**Fig. 7a-d**). Collectively, these data suggest that endogenous levels of single-strand DNA, as assessed by chromatin-bound RPA, can be utilized as a functional biomarker to predict enhancement in PARPi sensitivity upon ALC1 loss.

Discussion

Here, we define the clinical context in which targeting ALC1 can effectively overcome the clinical limitations of PARPi in the regimen of HGSOCs. We observe a profound impact of ALC1 depletion on PARPi responses in ovarian cancer cells with a *BRCA1/2*-mutation (**Fig. 2**), with high cyclin E1-levels, (**Fig. 3**) and with partial restoration of HR (**Fig. 4**). Our data suggests that targeting ALC1 can permit low PARPi dosage for an effective response, thereby potentially reducing therapy-associated side effects. Moreover, the expedited PARPi-mediated killing of cancer cells upon ALC1 also warrants that targeting this remodeler will likely be more beneficial in a frontline setting to mitigate the acquisition of resistance. This notion is also supported by our observations that ALC1 depletion has modest impact in contexts where PARPi resistance has been acquired by overexpression of full length BRCA1.

Many factors previously identified to enhance PARPi sensitivity, such as XRCC1, Fanconi anemia protein (FA), Rad51 and Rad54 paralogs, do so both in cancer and non-cancer cell lines[40]. This is in part due to the roles of these proteins in either single-strand or HR repair and hence a compromise in the front-line repair mechanisms, resulting in enhanced sensitivity both in cancer and non-cancer cells. Similarly, while inhibitors of checkpoint kinase ATR or Chk1 synergize with PARPi in killing HGSOCs, their critical roles in DNA replication impose the risk of unwanted pathological phenotypes in normal healthy cells[41]. In contrast, we demonstrate that ALC1 targeting is likely to have minimal impact on genome stability and PARPi sensitivity of normal fallopian tube epithelial cells (**Fig. 5,6**). These data uncover the unique potential of ALC1 targeting in significantly expanding the therapeutic index of PARPi.

This distinction in the impact of ALC1 on cancer versus non-cancer cells prompted us to examine the endogenous vulnerability that is exploited upon ALC1 loss for enhanced PARPi response. We recently reported that PARPi hypersensitivity upon ALC1 loss is reliant on presence of abasic sites. Abasic sites can arise spontaneously in cells upon the loss of nitrogen bases, a process which tends to be four times higher in the context of single-stranded DNA compared to its double-stranded counterpart. We therefore speculate that increased single-stranded DNA can directly correlate with increased PARPi sensitivity upon ALC1 loss. Indeed, we observe that levels of single-stranded DNA, as quantified by levels of chromatin-bound RPA, can be used as a predictor of enhanced PARPi response upon ALC1 depletion (**Fig.7**). This observation could explain why HR-proficient cyclin E1-high cells, which experience elevated replication stress and consequently accumulate more single stranded DNA, become sensitized to PARPi when ALC1 is depleted.

Our findings that ALC1 selectively sensitizes to PARPi but not platinum-based drugs highlight the distinction in determinants of the responses to the two therapies frequently used in the regimen of HGSOCs. As per FDA mandate, PARPi are typically prescribed to individuals who show positive responses to platinum. However, our studies suggest that ALC1 targeting can allow platinum-resistant tumors to be sensitized to PARP inhibitors. This observation is particularly meaningful in the context of cyclin E1-high ovarian cancers that are inherently resistant to platinum-based therapies.

When implementing synergistic combinations, it is likely that not all PARPi will behave the same. Our studies simultaneously comparing the impact of available inhibitors that trap PARP1/2 enzymes reveal that moderate trappers, olaparib and rucaparib, are likely to be more favorable in combinatorial therapy. We also show that ALC1 targeting in *BRCA1*-mutant cancers can permit the utility of veliparib, which is a safer PARPi and also can be effective in situations where tumors have acquired resistance owing to activation of multi-drug efflux pumps[42]. In contrast, in ovarian cancers that have acquired PARPi resistance due to overexpression of *BRCA1/2* protein, ALC1 targeting can enhance sensitivity to talazoparib. Hence, our studies warrant that in the context of combinatorial strategies, responses across PARPi can widely vary, and this should be an important clinical consideration.

We recognize that our studies are performed using ALC1 depletion and not small molecule inhibitors of ALC1, which are not commercially available. Hence, the relevance of our findings will be more pronounced in scenarios where an inhibitor abrogates ALC1 function without increasing its trapping onto the chromatin. In future studies, it will be imperative to examine how trapping versus non-trapping inhibitors of ALC1 can impact the therapeutic efficacy of this promising drug target.

METHODS

Immunohistochemistry (IHC) Staining. Tissue microarray studies were conducted on surgically resected high-grade serous ovarian cancer specimens from 78 patients diagnosed at the Department of Pathology at Washington University (St. Louis, MO, USA). All 5 tissue microarray slides were stained, imaged, and analyzed in parallel to minimize technical variability. Slides were pretreated for staining with a 45-minute bake step and a 12-minute dewax step, followed by 20 minutes of antigen retrieval in citrate buffer at 95°C. Endogenous peroxidases were quenched in dilute hydrogen peroxide. Tissues underwent a 15-minute blocking step each with an Avidin D and Biotin blocking reagent (Vector Labs, SP-2001), followed by a 5-minute blocking step with Protein Block Serum-Free (Dako, X0909). Tissues were then incubated with Anti-CHD1L antibody (Sigma-Aldrich, HPA028670) overnight at 4°C. After washing off the primary antibody, tissues were incubated with the secondary antibody (Vector Labs, BA-1000) for 30 minutes at room temperature, followed by an incubation with horseradish peroxidase (Vector Labs, SA-5004) for 30 minutes at 37°C. Tissue-bound immunocomplexes were detected by incubating with diaminobenzidine (Dako, K3468) for 5 minutes at room temperature. Finally, tissue sections were counterstained with hematoxylin (BioCare Medical, CATHE-M). Stained tissue sections were imaged with an AxioScan.Z1 whole tissue scanner and ZEN v2 software (Carl Zeiss). Unbiased parallelized analysis was then performed with HALO v3 digital pathology (Indica Labs). Section images were annotated to include tissue regions of interest and exclude artifacts and debris. For the "Area Quantification v2" analysis module, stain colors and thresholds were set and measured across all sections to calculate the percentage of stains within the annotated regions of interest.

Analysis of co-relation between ALC1 protein expression and PARPi response. Proteomic data was previously generated from laser microdissected enriched tumor material from HGSOC patients with HRD disease (Burdett et al Nature Genetics 2023). Of these cases, 9 patients had received PARPi treatment. A total of 65 tumor samples, collected at 3 timepoints (P= primary, R = relapse, A = autopsy), had proteomics data from these 9 patients (**Table 1**).

Cell Culture. UWB1.289, UWB1,289+BRCA1, hTERT FT282, hTERT FT190, hTERT FT194, OVCAR3, OVCAR4, and OVCAR8 were procured from ATCC. OVSAHO cells were obtained from Sigma. UWB1.289 cells, including the derivative SYr12, SYr14, RR, and BRCA1-add back variants, were cultured in 1:1 Mammary Epithelial Cell Basal Medium (Thermo Fisher Scientific, M-171) and RPMI1640 with L-glutamine (Genesee Scientific, 25-506) supplemented with Mammary Epithelial Growth Supplement (Thermo Fisher Scientific, S0155), 10% fetal bovine serum (FBS) (Sigma, F0926), and 1x Penicillin-Streptomycin (P/S) (Genesee Scientific 25-512). OVSAHO, OVCAR8, and primary cell lines (AOCS) were cultured in RPMI1640 with L-glutamine (Genesee Scientific, 25-506) supplemented with 10% FBS and 1x P/S. OVCAR3 and OVCAR4 cells were cultured in RPMI1640 with L-glutamine (Genesee Scientific, 25-506) supplemented with 10% FBS, 1x P/S, and 0.5% insulin (Thermo Fisher Scientific, ITS-G 100X). hTERT FT190, hTERT 194, hTERT FT282, and FT282 BRCA1 heterozygous cells were cultured in DMEM/F-12 with L-glutamine (Sigma D8062) supplemented with 10% bovine calf serum (BCS) (Cytiva, SH30072.04) and 1x P/S.

Lentivirus Transduction. HEK293T cells were used to produce lentiviruses. In a 6-well plate, HEK293T cells were transfected using Opti-MEM (Thermo Fisher Scientific, 31985070) solution containing 3750ng PAX2, 2500ng VSVG, 5250ng plasmid of interest, and 40uL of 1mg/mL polyethylenimine. 7 hours post - transfection, the media was changed. Lentivirus was collected 4 times over the course of 3 days, then stored

at -80˚C until time of use. Cells were transduced with lentivirus and 8ug/mL polybrene, followed by centrifugation at 600xg for 30 minutes to increase infection efficiency. 24 hours post-transduction, the media was changed. 48 hours post-transduction, a selection drug was added (Puromycin 2ug/mL or Blasticidin 5ug/mL).

sgRNAs used in the study. The 2-in-1 SaCas9 system was used to deplete ALC1 for most of the cell viability studies. The two-vector SpCas9 system was used for depleting ALC1 and pol theta in the MMEJ reporter assay. These sgRNAs have previously been validated for target specificity. Nucleofection of guides with recombinant Cas9 protein was used to generate BRCA1 heterozygous FT282 cells. The sgRNAs used in the study are:

SaCas9-sg*ALC1*: 5'TCCACAACAAGAACACTCCAA 3'

SaCas9-sg*AAVS1*: 5' GGTTCTGGGAGAGGGTAGCG 3'

SpCas9-sg*BRCA1*: 5' TAAATCTCGTACTTTCTTGT 3'

SpCas9-sg*ALC1*: 5' GTCGCCTGCATATGTTACAC 3'

SpCas9-sg*Pol theta:* 5' ACTCCGACGCAGAAGATTCA 3'

SpCas9-sg*AAVS1:* 5' GGGGCCACTAGGGACAGGAT 3'

Immunoblotting. Cell pellets were lysed by incubation with a 5x volume of radioimmunoprecipitation assay (RIPA) buffer supplemented with 1mM dithiothreitol (DTT), 1x complete EDTA-free protease inhibitor cocktail (Sigma, 11873580001), 0.5uL benzonase (EMD Millipore, 70746-3), and 1mM phenylmethylsulfonyl fluoride (PMSF) for 20 minutes on ice. The cell suspension was then centrifuged at 4˚C for 20 minutes to separate the supernatant from the cell debris. Bradford assay was used to quantify the protein concentration in the supernatant. 10-20ug of protein lysate was run on a Nupage 4-12% Tris protein gel (Thermo Fisher Scientific, NP0336) in 1x 3-(N-morpholino) propanesulfonic acid (MOPS) buffer. Protein was then transferred to a 0.2micron nitrocellulose membrane (Cytiva, 10600004) using a wet transfer at 400mA for 2 hours. Blocking was done in 5% milk in PBS with 0.2% Tween for 1 hour. Blots were incubated overnight with primary antibodies at 4˚C. The next day, blots were then washed 4 times with 0.2% Tween in PBS. Blots were next probed with HRP-conjugated secondary antibody at 1:3000 at room temperature for 1 hour, followed by 4 washes with 0.2% Tween in PBS. The Western lighting Plus ECL kit (Perkin Elmer, NEL10500) was used to develop the blot, followed by imaging on the iBright CL1500 Imaging system (Thermo Fisher Scientific, A44240). The details of primary and secondary antibodies are listed in **Table 2**.

Cell Viability Assays. For all cell viability assays, sgRNA depletion of ALC1 or AAVS1 was completed 2 weeks prior to plating. For each cell type, 1000 cells in a volume of 100uL were plated in a 96-well plate in technical triplicates. UWB1.289, including SYr12, SYr14, del 11q, and BRCA1+ variants, JHOS-4, OVSAHO, and primary cells (AOCS) were plated in white 96-well plates (Alkali Scientific TPW90960). hTERT FT190, hTERT FT194, hTERT FT282 BRCA1 WT and heterozygous, OVCAR3, OVCAR4, and OVCAR8 cells were plated in clear 96-well plates. 24 hours after cells were plated, 100uL of 2x drug dilutions were added. For HR-proficient cell lines, viability was assessed 1 week after cells were plated. For HR-deficient cell lines, viability was assessed 1 week after drugs were added to the cells. Cell lines that were plated in clear 96-well plates were assessed using the Resazurin fluorescence assay. Accordingly, on

the day of viability assessment, media was replaced with phenol red-free DMEM (Thermo Fisher Scientific, 31053028) supplemented with 10% bovine calf serum (BCS) (Cytiva, SH30072.04), 1x Penicillin Streptomycin, 2mM L-glutamine (Sigma D8062), and 10µg/ml resazurin (Sigma, 199303). Cells were incubated for 3-4 hours at 37˚C in resazurin-containing media, followed by fluorescence measurement. Fluorescence was measured using the SoftMax Pro 6.4 software on the SpectraMax i3x microplate reader on 560nm excitation and 590nm emission settings. Cell lines that were plated in white 96-well plates were assessed using CellTiter Glo 2.0 Assay (Promega, PRG9242). Luminescence was measured on the aforementioned microplate reader on the luminescence setting. Fluorescence or luminescence of the drug-treated population was normalized to its respective untreated control, then survival curves were plotted. GraphPad Prism was used to fit the data to a curve via the following equation: $y = min + (max – min) / 1 + 10^{logEC50-x}$.

Microhomology-mediated End Joining (MMEJ) Reporter Assay. The MMEJ reporter assay was conducted following a published protocol. Briefly, HEK293T cells were engineered to stably express an I-SceI site containing an MMEJ-dependent mCherry reporter. These cells were then transduced with lentivirus expressing single guide RNA for *ALC1*, *Polymerase Theta*, or *AAVS1* control, then selected using Blastcidin. After 2 weeks of depletion, $0.05x10^6$ cells were plated in each well of a 24-well plate. The following day, cells were then transfected with the I-Sce I enzyme plasmid with a BFP reporter using the Lipofectamine 3000 kit, according to the manufacturer's instructions (Thermo Fisher, L3000008). After 3 days of transfection, cells were collected and analyzed via flow cytometry for BFP and mCherry expression. The BFP+ population (cells that express the I-SceI plasmid) was gated on to quantify the percentage of mCherry expression (cells that successfully performed MMEJ).

Immunofluorescence Staining. For each cell type, 25,000 cells were plated on poly-lysine-coated coverslips in a 24-well plate. Cells were given 48 hours to attach to the coverslips. For RAD51 foci formation experiments, cells were then treated for 24 hours with 10µM olaparib. Cells were pulse-labelled with 1ug/mL 5-Ethynyl-2'-deoxyuridine (EdU) for 20 minutes to label replicating cells. Following EdU labelling, cells were pre-extracted on ice for 5 minutes with ice-cold cytoskeleton buffer (10 mM Pipes pH 6.8, 100 mM NaCl, 300 mM sucrose, 3mM $MgCl_2$, 1mM EGTA, 0.5% Triton X-100) and then fixed with 3% paraformaldehyde (PFA) for 15minutes at room temperature. Four PBS washes were done to remove residual PFA following fixation. Cells were then permeabilized on ice for 5 minutes with 0.5% Triton-X in PBS, followed by blocking in 3% bovine serum albumin (BSA) dissolved in PBS. Incorporated EdU was labeled with Alexa-Fluor-647 Azide using the Click Reaction denoted in the manufacturer's instructions (Fisher Scientific, 502108139). Cells were then washed once with blocking buffer, 3 times with PBST, and once with PBS. Cells were fixed again with 3% PFA for 10 minutes at room temperature, then washed four times with PBST. For RAD51 staining, samples were incubated overnight at 4˚C with rabbit-anti-RAD51 (ABCAM, ab63801) diluted 1:250 and mouse-anti-γH2AX (Sigma-Aldrich, 05-636) diluted 1:1000 in DMEM media with 0.02% sodium azide. For γH2AX and RPA32 or pS33-RPA32 staining, cell samples were incubated for 1 hour at room temperature with mouse-anti-γH2AX (Sigma-Aldrich, 05-636) diluted 1:1000 and rabbit-anti-RPA32 (Cell Signaling, 35869S) or rabbit-anti-RPA32-S33 (Thermo Fisher Scientific, A300-246A) diluted 1:500 in DMEM media with 0.02% sodium azide. Following four washes with PBST, samples were incubated for 1 hour at room temperature with Alexa-Fluor-555-conjugated anti-mouse (Thermo Fisher Scientific, A32773) and Alexa-Fluor-488-conjugated anti-rabbit (Thermo Fisher Scientific, A32731) secondary antibodies, each diluted 1:1000 in DMEM media with azide. Following four washes with PBST and four washes with MQ water, samples were incubated for 2 minutes at room

temperature with 1 μg/mL 4',6-diamidino-2-phenylindole (DAPI) made in MQ water. Coverslips were mounted using Vectashield Vibrance Antifade Mounting Medium (Vector Labs, H-1700). Images were acquired using a Nikon Ti-2 microscope with a 60x objective. Z-stacks were imaged every 0.2 microns, followed by deconvolution and extended depth focus analysis to visualize 3D projections. Analysis was done using the Nikon GA3 processing tool, in which cells were defined in the DAPI channel. γH2AX, RAD51, RPA32, or RPA32-S33 foci were quantified in an automated fashion for each cell using the Nikon GA3 BrightSpot function.

Xenograft studies. Xenograft studies were carried out under protocol no. 24-0237 approved by the Institutional Animal Care & Use Committee at the Washington University, School of Medicine. Six-week-old female NU/J mice were procured from Jackson Mice. Laboratory tumor implantation was performed once these mice were seven to eight weeks old. OVCAR8 cells were engineered to stably express a 2-in-1 SaCas9 plasmid expressing either sg*AAVS1* or sg*ALC1*. 3×10^6 cells mixed 1:1 with Matrigel (Fisher Scientific, cat. no. 356237) were injected intraperitoneally into the mice. 14 days post-tumor implantation, two mice in each group were sacrificed to ensure the initiation of tumor nodules. 10 mice per group were randomized into vehicle- and drug-treated groups. Olaparib (selleckchem) was dissolved in captisol to a concentration of $50\,\mathrm{mg\,ml^{-1}}$. A $50\,\mathrm{mg\,kg^{-1}}$ dose of the drug was administered every second day for 35 days. At 35 days post-initiation of treatment, mice were sacrificed and analyzed for tumor weights and nodules.

Contributions

P.V. and M.M. conceived the idea and secured the funding. L.N.A and D.H.W. pursued most of the experiments, N.M.R. optimized and performed the MMEJ reporter assay, R.R. and D.K. assisted in qualitative immunofluorescence imaging, K.E.J. and V.M. helped with immunoblotting, and K.Z. helped with cloning under the supervision of P.V. A.C. and E.L. performed the xenograft experiments and helped with IHC studies under the supervision of M.M. D.K. provided the TMA. E.L.C. analyzed the patient proteomics data. P.V., L.N.A., and N.M.R. wrote the manuscript with contributions from all other authors.

Acknowledgements

We thank Dr. Alessandro Vindigni and the Genome Engineering and iPSC Center (GEiC) at the Washington University in St. Louis for the generation and validation of BRCA1 het FT282 cell lines. UWB SYr12 and SYr14 cell lines were obtained from Dr. Lee Zou at Duke University, School of Medicine. JHOS-4 and UWB-RR cell lines were obtained from Dr. John Krais and Dr. Neil Johnson at Fox Chase Cancer Center. MMEJ reporter plasmids were provided by Dr. Nausica Arnoult at UC, Boulder. This work was supported by the Inaugural Pedal the Cause Grant by Alvin J. Siteman Cancer Center through The Foundation for Barnes-Jewish Hospital, V-Scholar grant, Early-career investigator Award from Ovarian Cancer Research Fund Alliance, Career Catalyst Grant from Susan G. Komen and R37-CA286908 to P.V., who is also supported by Early-career Investigator Award from Ovarian Cancer Academy, Department of Defense, The Victoria's Secret Global Fund for Women's Cancers Career Development Award, in

partnership with Pelotonia and the AACR and pilot project grant from Longer Life Foundation. L.N.A. is supported by the NIH Cancer Biology Pathway training T32 grant to Washington University, St. Louis.

References

1. Siegel, R.L., Miller, K.D., Wagle, N.S., and Jemal, A. (2023). Cancer statistics, 2023. CA Cancer J Clin *73*, 17–48.

2. Patch, A.-M., Christie, E.L., Etemadmoghadam, D., Garsed, D.W., George, J., Fereday, S., Nones, K., Cowin, P., Alsop, K., Bailey, P.J., et al. (2015). Whole-genome characterization of chemoresistant ovarian cancer. Nature *521*, 489–494.

3. Dias, M.P., Moser, S.C., Ganesan, S., and Jonkers, J. (2021). Understanding and overcoming resistance to PARP inhibitors in cancer therapy. Nat Rev Clin Oncol *18*, 773–791.

4. Morice, P.-M., Leary, A., Dolladille, C., Chrétien, B., Poulain, L., González-Martín, A., Moore, K., O'Reilly, E.M., Ray-Coquard, I., and Alexandre, J. (2021). Myelodysplastic syndrome and acute myeloid leukaemia in patients treated with PARP inhibitors: a safety meta-analysis of randomised controlled trials and a retrospective study of the WHO pharmacovigilance database. Lancet Haematol. *8*, e122–e134.

5. Rosen, D.G., Yang, G., Deavers, M.T., Malpica, A., Kavanagh, J.J., Mills, G.B., and Liu, J. (2006). Cyclin E expression is correlated with tumor progression and predicts a poor prognosis in patients with ovarian carcinoma. Cancer *106*, 1925–1932.

6. Murai, J., Huang, S.-Y.N., Das, B.B., Renaud, A., Zhang, Y., Doroshow, J.H., Ji, J., Takeda, S., and Pommier, Y. (2012). Trapping of PARP1 and PARP2 by clinical PARP inhibitors. Cancer Res. *72*, 5588–5599.

7. Chornenkyy, Y., Agnihotri, S., Yu, M., Buczkowicz, P., Rakopoulos, P., Golbourn, B., Garzia, L., Siddaway, R., Leung, S., Rutka, J.T., et al. (2015). Poly-ADP-Ribose Polymerase as a Therapeutic Target in Pediatric Diffuse Intrinsic Pontine Glioma and Pediatric High-Grade Astrocytoma. Mol Cancer Ther *14*, 2560–2568.

8. Slade, D. (2020). PARP and PARG inhibitors in cancer treatment. Genes Dev *34*, 360–394.

9. Verma, P., Zhou, Y., Cao, Z., Deraska, P.V., Deb, M., Arai, E., Li, W., Shao, Y., Puentes, L., Li, Y., et al. (2021). ALC1 links chromatin accessibility to PARP inhibitor response in homologous recombination-deficient cells. Nat. Cell Biol. *23*, 160–171.

10. Hewitt, G., Borel, V., Segura-Bayona, S., Takaki, T., Ruis, P., Bellelli, R., Lehmann, L.C., Sommerova, L., Vancevska, A., Tomas-Loba, A., et al. (2021). Defective ALC1 nucleosome remodeling confers PARPi sensitization and synthetic lethality with HRD. Mol Cell *81*, 767–783.e11.

11. Ramakrishnan, N., Weaver, T.M., Aubuchon, L.N., Woldegerima, A., Just, T., Song, K., Vindigni, A., Freudenthal, B.D., and Verma, P. (2024). Nucleolytic processing of abasic sites underlies PARP inhibitor hypersensitivity in ALC1-deficient BRCA mutant cancer cells. Nat. Commun. *15*, 6343.

12. Aubuchon, L.N., and Verma, P. (2024). Endogenous base damage as a driver of genomic instability in homologous recombination-deficient cancers. DNA Repair (Amst.) *141*, 103736.

13. Cerami, E., Gao, J., Dogrusoz, U., Gross, B.E., Sumer, S.O., Aksoy, B.A., Jacobsen, A., Byrne, C.J., Heuer, M.L., Larsson, E., et al. (2012). The cBio cancer genomics portal: an open platform for exploring multidimensional cancer genomics data. Cancer Discov *2*, 401–404.

14. Győrffy, B. (2023). Discovery and ranking of the most robust prognostic biomarkers in serous ovarian cancer. Geroscience *45*, 1889–1898.

15. Burdett, N.L., Willis, M.O., Alsop, K., Hunt, A.L., Pandey, A., Hamilton, P.T., Abulez, T., Liu, X., Hoang, T., Craig, S., et al. (2023). Multiomic analysis of homologous recombination-deficient end-stage high-grade serous ovarian cancer. Nat Genet *55*, 437–450.

16. Ceccaldi, R., Liu, J.C., Amunugama, R., Hajdu, I., Primack, B., Petalcorin, M.I.R., O'Connor, K.W., Konstantinopoulos, P.A., Elledge, S.J., Boulton, S.J., et al. (2015). Homologous-recombination-deficient tumours are dependent on Polθ-mediated repair. Nature *518*, 258–262.

17. Mateos-Gomez, P.A., Gong, F., Nair, N., Miller, K.M., Lazzerini-Denchi, E., and Sfeir, A. (2015). Mammalian polymerase θ promotes alternative NHEJ and suppresses recombination. Nature *518*, 254–257.

18. Fleury, H., MacEachern, M.K., Stiefel, C.M., Anand, R., Sempeck, C., Nebenfuehr, B., Maurer-Alcalá, K., Ball, K., Proctor, B., 3rd, Belan, O., et al. (2023). The APE2 nuclease is essential for DNA double-strand break repair by microhomology-mediated end joining. Mol Cell *83*, 1429–1445.e8.

19. Cleary, J.M., Aguirre, A.J., Shapiro, G.I., and D'Andrea, A.D. (2020). Biomarker-Guided Development of DNA Repair Inhibitors. Mol Cell *78*, 1070–1085.

20. Karst, A.M., Jones, P.M., Vena, N., Ligon, A.H., Liu, J.F., Hirsch, M.S., Etemadmoghadam, D., Bowtell, D.D.L., and Drapkin, R. (2014). Cyclin E1 deregulation occurs early in secretory cell transformation to promote formation of fallopian tube-derived high-grade serous ovarian cancers. Cancer Res *74*, 1141–1152.

21. Kang, E.-Y., Weir, A., Meagher, N.S., Farrington, K., Nelson, G.S., Ghatage, P., Lee, C.-H., Riggan, M.J., Bolithon, A., Popovic, G., et al. (2023). CCNE1 and survival of patients with tubo-ovarian high-grade serous carcinoma: An Ovarian Tumor Tissue Analysis consortium study. Cancer *129*, 697–713.

22. Xu, H., George, E., Kinose, Y., Kim, H., Shah, J.B., Peake, J.D., Ferman, B., Medvedev, S., Murtha, T., Barger, C.J., et al. (2021). copy number is a biomarker for response to combination WEE1-ATR inhibition in ovarian and endometrial cancer models. Cell Rep Med *2*, 100394.

23. Jones, R.M., Mortusewicz, O., Afzal, I., Lorvellec, M., García, P., Helleday, T., and Petermann, E. (2013). Increased replication initiation and conflicts with transcription underlie Cyclin E-induced replication stress. Oncogene *32*, 3744–3753.

24. Kok, Y.P., Guerrero Llobet, S., Schoonen, P.M., Everts, M., Bhattacharya, A., Fehrmann, R.S.N., van den Tempel, N., and van Vugt, M.A.T.M. (2020). Overexpression of Cyclin E1 or Cdc25A leads to replication stress, mitotic aberrancies, and increased sensitivity to replication checkpoint inhibitors. Oncogenesis *9*, 88.

25. Mitra, A.K., Davis, D.A., Tomar, S., Roy, L., Gurler, H., Xie, J., Lantvit, D.D., Cardenas, H., Fang, F., Liu, Y., et al. (2015). In vivo tumor growth of high-grade serous ovarian cancer cell lines.

Gynecol Oncol *138*, 372–377.

26. Yazinski, S.A., Comaills, V., Buisson, R., Genois, M.-M., Nguyen, H.D., Ho, C.K., Todorova Kwan, T., Morris, R., Lauffer, S., Nussenzweig, A., et al. (2017). ATR inhibition disrupts rewired homologous recombination and fork protection pathways in PARP inhibitor-resistant BRCA-deficient cancer cells. Genes Dev *31*, 318–332.

27. Wethington, S.L., Shah, P.D., Martin, L., Tanyi, J.L., Latif, N., Morgan, M., Torigian, D.A., Rodriguez, D., Smith, S.A., Dean, E., et al. (2023). Combination ATR (ceralasertib) and PARP (olaparib) Inhibitor (CAPRI) Trial in Acquired PARP Inhibitor-Resistant Homologous Recombination-Deficient Ovarian Cancer. Clin Cancer Res *29*, 2800–2807.

28. Wang, Y., Krais, J.J., Bernhardy, A.J., Nicolas, E., Cai, K.Q., Harrell, M.I., Kim, H.H., George, E., Swisher, E.M., Simpkins, F., et al. (2016). RING domain-deficient BRCA1 promotes PARP inhibitor and platinum resistance. J Clin Invest *126*, 3145–3157.

29. Drost, R., Dhillon, K.K., van der Gulden, H., van der Heijden, I., Brandsma, I., Cruz, C., Chondronasiou, D., Castroviejo-Bermejo, M., Boon, U., Schut, E., et al. (2016). BRCA1185delAG tumors may acquire therapy resistance through expression of RING-less BRCA1. J Clin Invest *126*, 2903–2918.

30. Park, P.H., Yamamoto, T.M., Li, H., Alcivar, A.L., Xia, B., Wang, Y., Bernhardy, A.J., Turner, K.M., Kossenkov, A.V., Watson, Z.L., et al. (2020). Amplification of the Mutation-Carrying BRCA2 Allele Promotes RAD51 Loading and PARP Inhibitor Resistance in the Absence of Reversion Mutations. Mol Cancer Ther *19*, 602–613.

31. Wang, Y., Bernhardy, A.J., Cruz, C., Krais, J.J., Nacson, J., Nicolas, E., Peri, S., van der Gulden, H., van der Heijden, I., O'Brien, S.W., et al. (2016). The BRCA1-Δ11q Alternative Splice Isoform Bypasses Germline Mutations and Promotes Therapeutic Resistance to PARP Inhibition and Cisplatin. Cancer Res *76*, 2778–2790.

32. Johnson, N., Johnson, S.F., Yao, W., Li, Y.-C., Choi, Y.-E., Bernhardy, A.J., Wang, Y., Capelletti, M., Sarosiek, K.A., Moreau, L.A., et al. (2013). Stabilization of mutant BRCA1 protein confers PARP inhibitor and platinum resistance. Proc Natl Acad Sci U S A *110*, 17041–17046.

33. DelloRusso, C., Welcsh, P.L., Wang, W., Garcia, R.L., King, M.-C., and Swisher, E.M. (2007). Functional characterization of a novel BRCA1-null ovarian cancer cell line in response to ionizing radiation. Mol Cancer Res *5*, 35–45.

34. Perets, R., Wyant, G.A., Muto, K.W., Bijron, J.G., Poole, B.B., Chin, K.T., Chen, J.Y.H., Ohman, A.W., Stepule, C.D., Kwak, S., et al. (2013). Transformation of the fallopian tube secretory epithelium leads to high-grade serous ovarian cancer in Brca;Tp53;Pten models. Cancer Cell *24*, 751–765.

35. Karst, A.M., and Drapkin, R. (2012). Primary culture and immortalization of human fallopian tube secretory epithelial cells. Nat Protoc *7*, 1755–1764.

36. Abkevich, V., Timms, K.M., Hennessy, B.T., Potter, J., Carey, M.S., Meyer, L.A., Smith-McCune, K., Broaddus, R., Lu, K.H., Chen, J., et al. (2012). Patterns of genomic loss of heterozygosity predict homologous recombination repair defects in epithelial ovarian cancer. Br J Cancer *107*, 1776–1782.

37. Pathania, S., Bade, S., Le Guillou, M., Burke, K., Reed, R., Bowman-Colin, C., Su, Y., Ting, D.T.,

Polyak, K., Richardson, A.L., et al. (2014). BRCA1 haploinsufficiency for replication stress suppression in primary cells. Nat Commun *5*, 5496.

38. Lim, P.X., Zaman, M., Feng, W., and Jasin, M. (2024). BRCA2 promotes genomic integrity and therapy resistance primarily through its role in homology-directed repair. Mol Cell *84*, 447–462.e10.

39. Lindahl, T., and Nyberg, B. (1972). Rate of depurination of native deoxyribonucleic acid. Biochemistry *11*, 3610–3618.

40. Zimmermann, M., Murina, O., Reijns, M.A.M., Agathanggelou, A., Challis, R., Tarnauskaitė, Ž., Muir, M., Fluteau, A., Aregger, M., McEwan, A., et al. (2018). CRISPR screens identify genomic ribonucleotides as a source of PARP-trapping lesions. Nature *559*, 285–289.

41. Karnitz, L.M., and Zou, L. (2015). Molecular Pathways: Targeting ATR in Cancer Therapy. Clin Cancer Res *21*, 4780–4785.

42. Rottenberg, S., Jaspers, J.E., Kersbergen, A., van der Burg, E., Nygren, A.O.H., Zander, S.A.L., Derksen, P.W.B., de Bruin, M., Zevenhoven, J., Lau, A., et al. (2008). High sensitivity of BRCA1-deficient mammary tumors to the PARP inhibitor AZD2281 alone and in combination with platinum drugs. Proc Natl Acad Sci U S A *105*, 17079–17084.

Figure 1

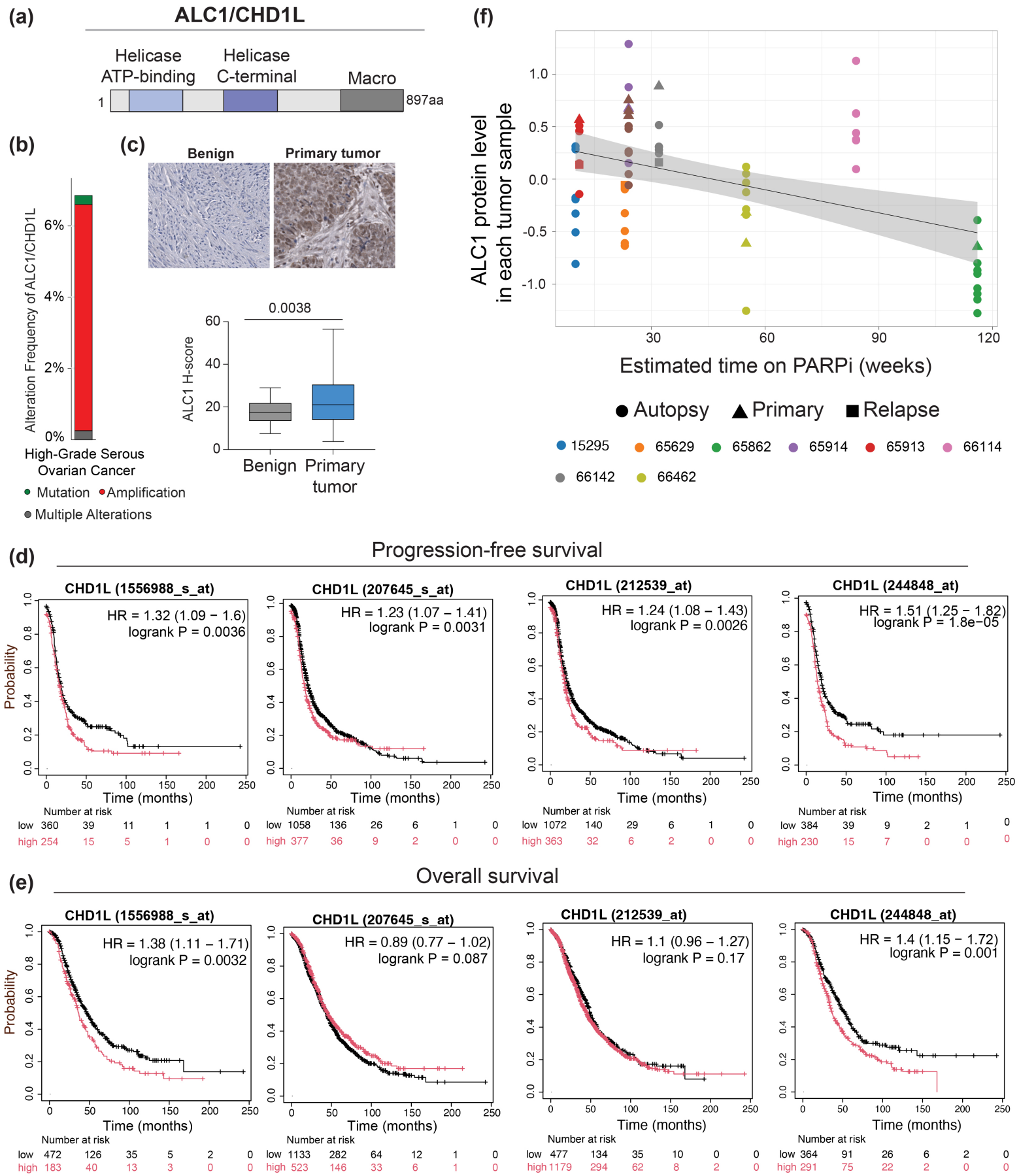
(a)
ALC1/CHD1L
Helicase ATP-binding
Helicase C-terminal
Macro
1
897aa
(b)
Alteration Frequency of ALC1/CHD1L
6%
4%
2%
0%
High-Grade Serous Ovarian Cancer
Mutation
Amplification
Multiple Alterations
(c)
Benign
Primary tumor
0.0038
ALC1 H-score
60
40
20
0
Benign
Primary tumor
(f)
ALC1 protein level in each tumor sample
1.0
0.5
0.0
-0.5
-1.0
30
60
90
120
Estimated time on PARPi (weeks)
Autopsy
Primary
Relapse
15295
65629
65862
65914
65913
66114
66142
66462
(d)
Progression-free survival
CHD1L (1556988_s_at)
HR = 1.32 (1.09 – 1.6)
logrank P = 0.0036
CHD1L (207645_s_at)
HR = 1.23 (1.07 – 1.41)
logrank P = 0.0031
CHD1L (212539_at)
HR = 1.24 (1.08 – 1.43)
logrank P = 0.0026
CHD1L (244848_at)
HR = 1.51 (1.25 – 1.82)
logrank P = 1.8e−05
Probability
Time (months)
Number at risk
low 360 39 11 1 1 0
high 254 15 5 1 0 0
low 1058 136 26 6 1 0
high 377 36 9 2 0 0
low 1072 140 29 6 1 0
high 363 32 6 2 0 0
low 384 39 9 2 1 0
high 230 15 7 0 0 0
(e)
Overall survival
CHD1L (1556988_s_at)
HR = 1.38 (1.11 – 1.71)
logrank P = 0.0032
CHD1L (207645_s_at)
HR = 0.89 (0.77 – 1.02)
logrank P = 0.087
CHD1L (212539_at)
HR = 1.1 (0.96 – 1.27)
logrank P = 0.17
CHD1L (244848_at)
HR = 1.4 (1.15 – 1.72)
logrank P = 0.001
Probability
Time (months)
Number at risk
low 472 126 35 5 2 0
high 183 40 13 3 0 0
low 1133 282 64 12 1 0
high 523 146 33 6 1 0
low 477 134 35 10 0 0
high 1179 294 62 8 2 0
low 364 91 26 6 2 0
high 291 75 22 2 0 0

Figure 1.

a. Schematic of human ALC1 protein; aa-amino acid.

b. Bar graph taken from cBioPortal showing alteration frequency in ALC1 in HGSOCs.

c. Representative image showing ALC1 protein expression in indicated tissues (top) and box-and-whisker plots showing quantification of ALC1 protein expression levels per H-scores in normal ovarian tissue (n=51 sites) and primary tumor (n=142 different sites) sampled from 78 patients. P-value is derived from Mann-Whitney test.

d. Curve derived from Kaplan–Meier plotter showing progression-free survival for high and low ALC1 expression across all ovarian tumor samples reported. High and low levels were determined by the software based on the best cutoff between the upper and the lower quartiles.

e. Curve derived from Kaplan–Meier plotter showing overall survival for high and low ALC1 expression across all ovarian tumor samples reported. High and low levels were determined by the software based on best cutoff between the upper and the lower quartiles.

f. Graph showing correlation with ALC1 protein levels and estimated time on PARPi. Due to the small size of the cohort, no statistical analysis was performed. The case number correspond to the IDs from Burdett *et al*, 2023[14].

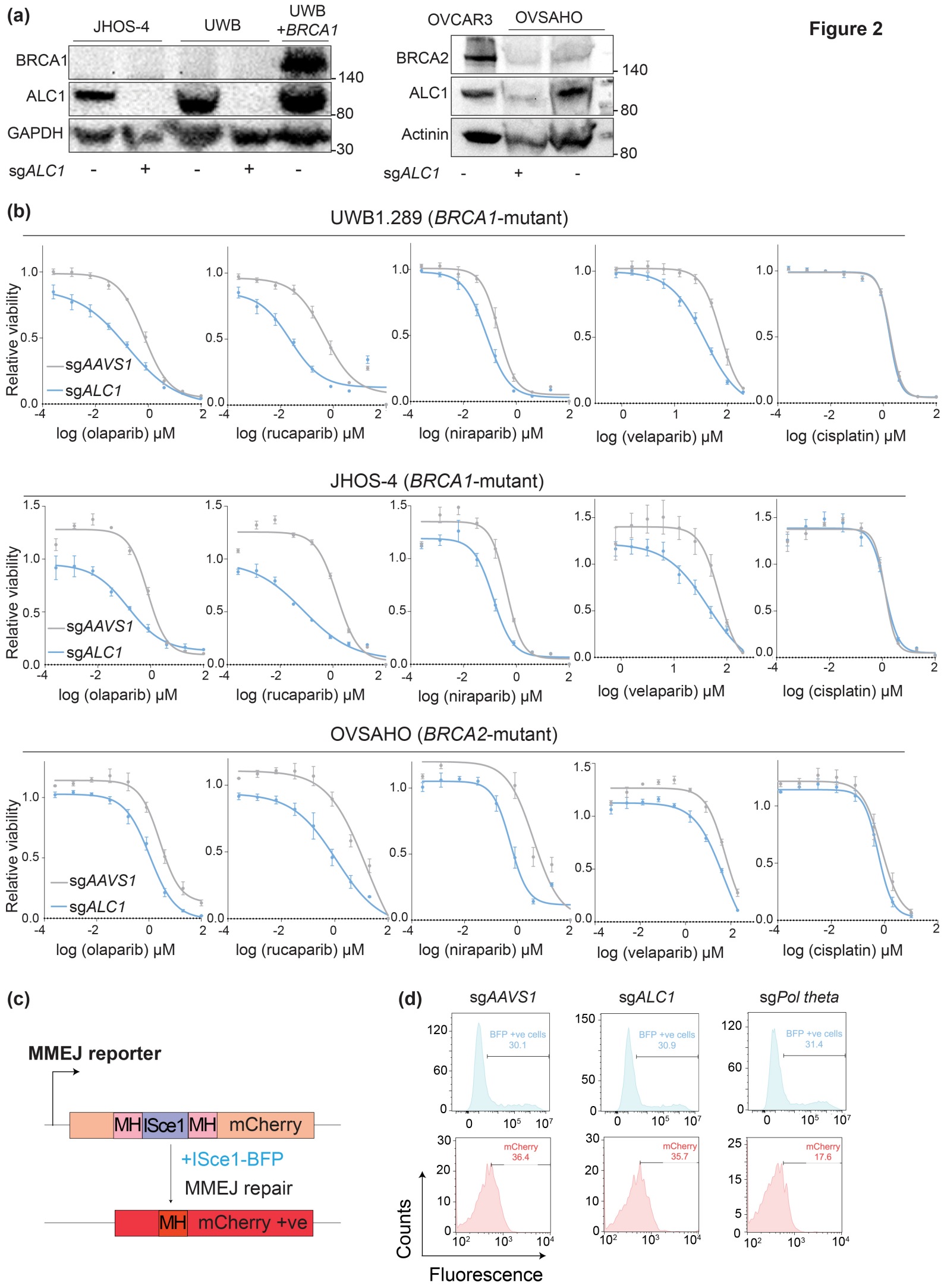

(a)
JHOS-4
UWB
UWB +BRCA1
BRCA1
ALC1
GAPDH
140
80
30
sgALC1 - + - + -
OVCAR3
OVSAHO
BRCA2
ALC1
Actinin
140
80
80
sgALC1 - + -
(b)
UWB1.289 (BRCA1-mutant)
JHOS-4 (BRCA1-mutant)
OVSAHO (BRCA2-mutant)
Relative viability
sgAAVS1
sgALC1
log (olaparib) μM
log (rucaparib) μM
log (niraparib) μM
log (velaparib) μM
log (cisplatin) μM
(c)
MMEJ reporter
MH
ISce1
MH
mCherry
+ISce1-BFP
MMEJ repair
MH
mCherry +ve
(d)
sgAAVS1
sgALC1
sgPol theta
BFP +ve cells 30.1
BFP +ve cells 30.9
BFP +ve cells 31.4
mCherry 36.4
mCherry 35.7
mCherry 17.6
Counts
Fluorescence

Figure 2

Figure 2. Loss of ALC1 enhances PARPi sensitivity across *BRCA1/2*-mutant ovarian cancer cell lines in a Microhomology-mediated end joining (MMEJ)-independent manner.

(a) Immunoblot showing ALC1 depletion levels in indicated cell lines.

(b) Sensitivities of the indicated *BRCA1/2*-mutated cell lines to various PARP inhibitors and Cisplatin using the CellTiter-Glo assay; n = 3 biologically independent experiments. Data are presented as mean ± s.e.m.

(c) Schematic of the MMEJ reporter assay. Cells are engineered to stably express a substrate that contains an ISec1-site flanked by microhomology (MH). Double-strand breaks can be induced via transfection of an ISec1-BFP plasmid. The repair of the break via MMEJ result in generation of mcherry signal which can be quantified using flow cytometry.

(d) Flow cytometry data showing transfection efficiency of ISec1 BFP plasmid (top) and MMEJ-mediated mcherry product formation (bottom) in HEK293T cells transfected with indicated sgRNAs.

Figure 3

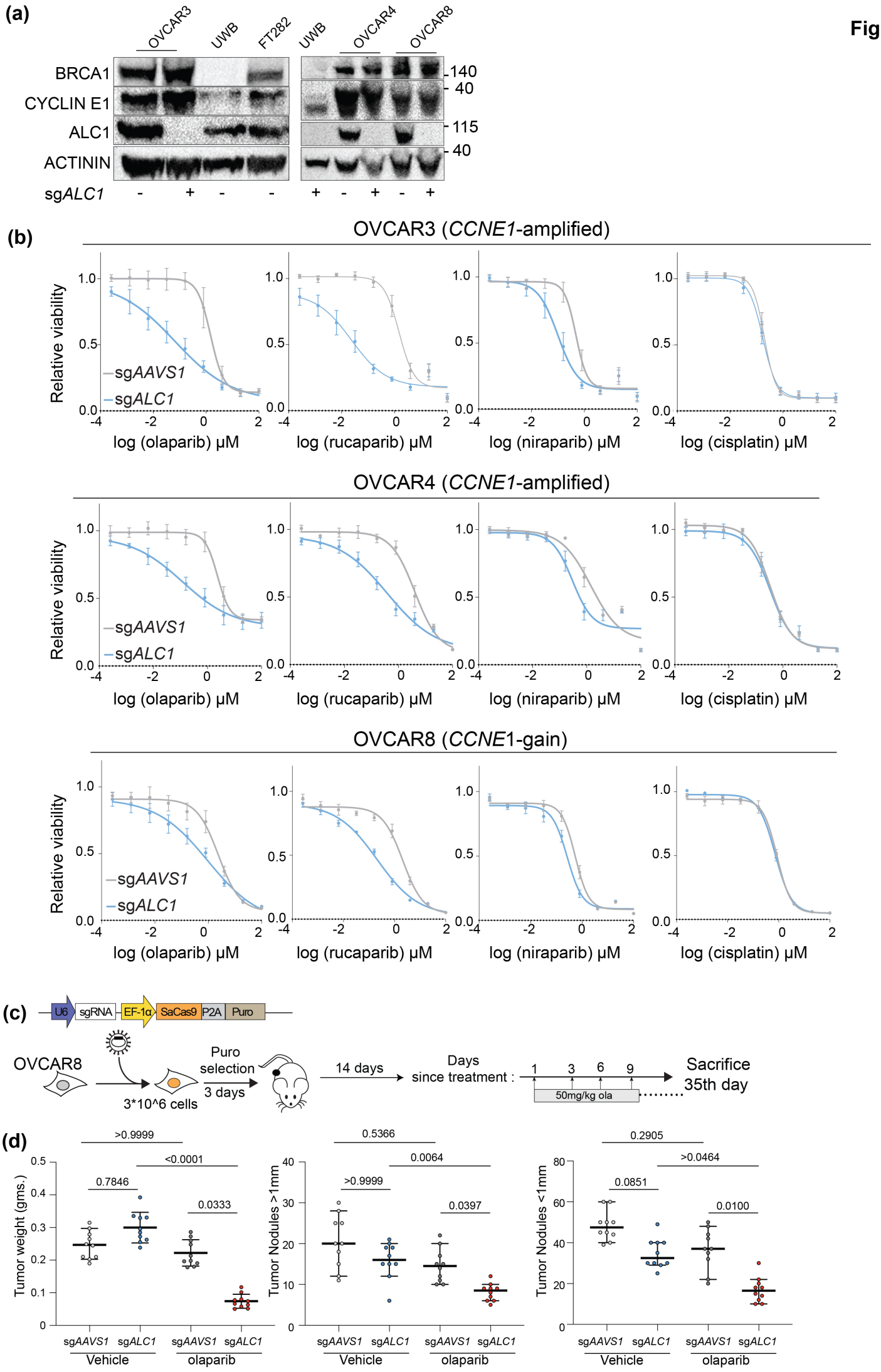
(a)
OVCAR3
UWB
FT282
UWB
OVCAR4
OVCAR8
BRCA1
CYCLIN E1
ALC1
ACTININ
sgALC1
140
40
115
40
(b)
OVCAR3 (CCNE1-amplified)
OVCAR4 (CCNE1-amplified)
OVCAR8 (CCNE1-gain)
Relative viability
sgAAVS1
sgALC1
log (olaparib) μM
log (rucaparib) μM
log (niraparib) μM
log (cisplatin) μM
(c)
U6
sgRNA
EF-1α
SaCas9
P2A
Puro
OVCAR8
3*10^6 cells
Puro selection
3 days
14 days
Days since treatment :
1
3
6
9
50mg/kg ola
Sacrifice 35th day
(d)
Tumor weight (gms.)
Tumor Nodules >1mm
Tumor Nodules <1mm
>0.9999
<0.0001
0.7846
0.0333
0.5366
0.0064
>0.9999
0.0397
0.2905
>0.0464
0.0851
0.0100
sgAAVS1
sgALC1
Vehicle
olaparib

Figure 3. ALC1 loss enhances PARPi sensitivity cyclin E1-high ovarian cancer cell lines and xenograft models.

(a) Immunoblot showing ALC1 depletion levels in indicated cyclin E1-high cell lines.

(b) Sensitivities of indicated cyclin E1-high cells to various PARPi and Cisplatin using the CellTiter-Glo assay; $n = 3$ biologically independent experiments. Data are presented as mean ± s.e.m.

(c) Schematic for the xenograft experiment.

(d) Assessment of tumor weight and nodules in indicated OVCAR8-derived xenografts. Mice were scarified at 35th day after initiation of PARPi treatment and indicated parameters were quantified. N=10/mice per group. P-value: Kruskal-Wallis test.

Figure 4

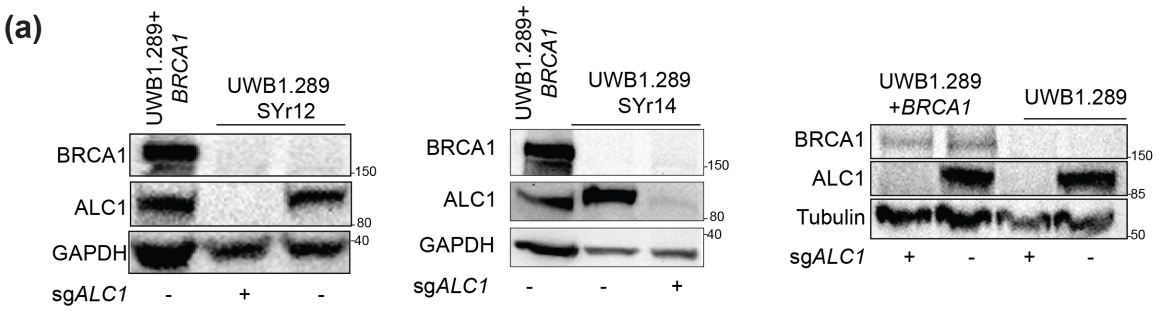
(a)
UWB1.289+ BRCA1
UWB1.289 SYr12
BRCA1
ALC1
GAPDH
sgALC1
150
80
40
UWB1.289+ BRCA1
UWB1.289 SYr14
UWB1.289 +BRCA1
UWB1.289
Tubulin
85
50

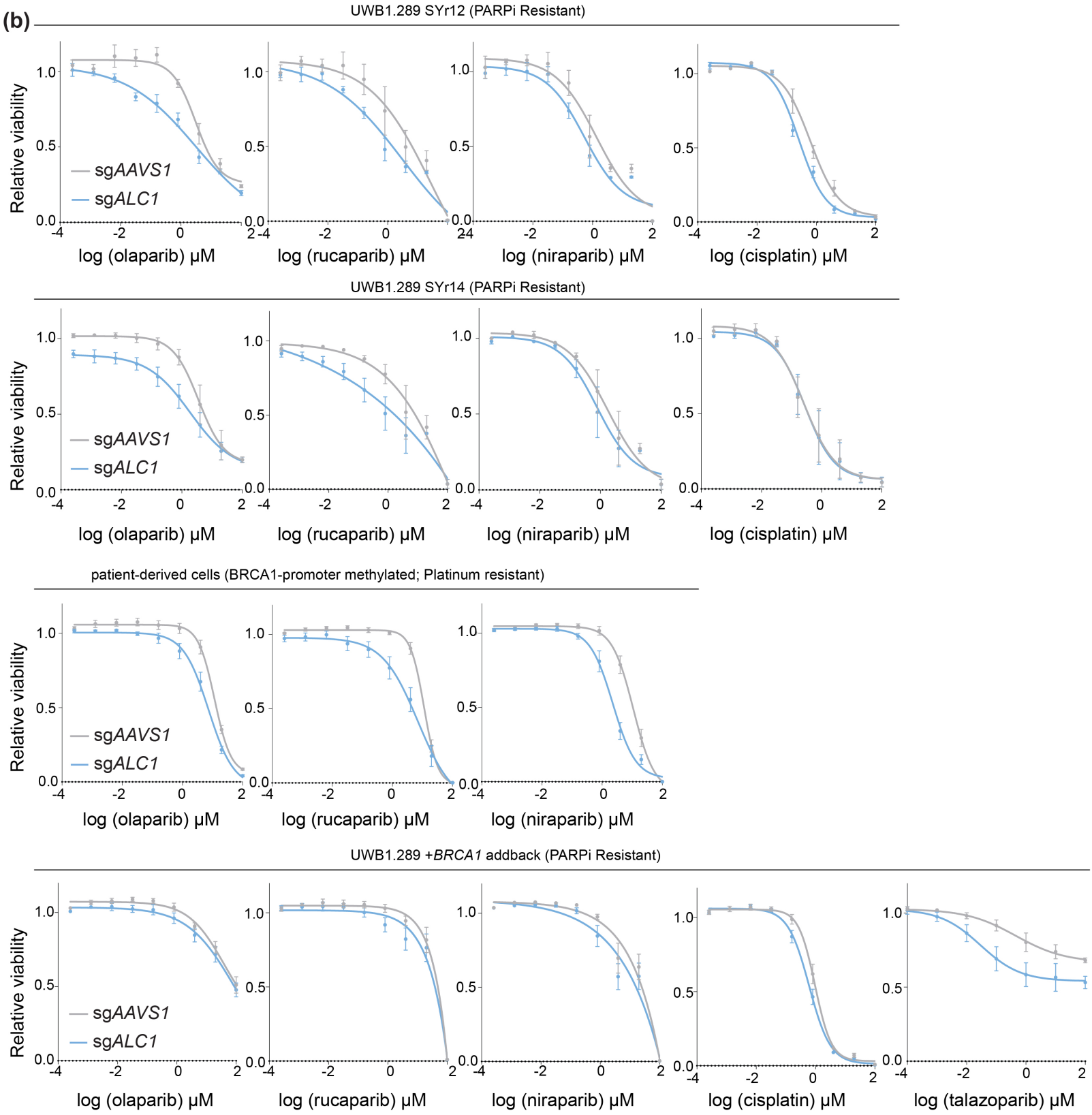
(b)
UWB1.289 SYr12 (PARPi Resistant)
UWB1.289 SYr14 (PARPi Resistant)
patient-derived cells (BRCA1-promoter methylated; Platinum resistant)
UWB1.289 +BRCA1 addback (PARPi Resistant)
Relative viability
sgAAVS1
sgALC1
log (olaparib) μM
log (rucaparib) μM
log (niraparib) μM
log (cisplatin) μM
log (talazoparib) μM

Figure 4. ALC1 loss restores PARPi sensitivity in ovarian cancer cell lines with partially restored homologous recombination.

(a) Immunoblot showing BRCA1 and ALC1 depletion levels in indicated cell lines.

(b) Sensitivities of indicated cells to various PARPi and Cisplatin using the CellTiter-Glo assay; $n = 3$ biologically independent experiments. Data are presented as mean ± s.e.m..

Figure 5

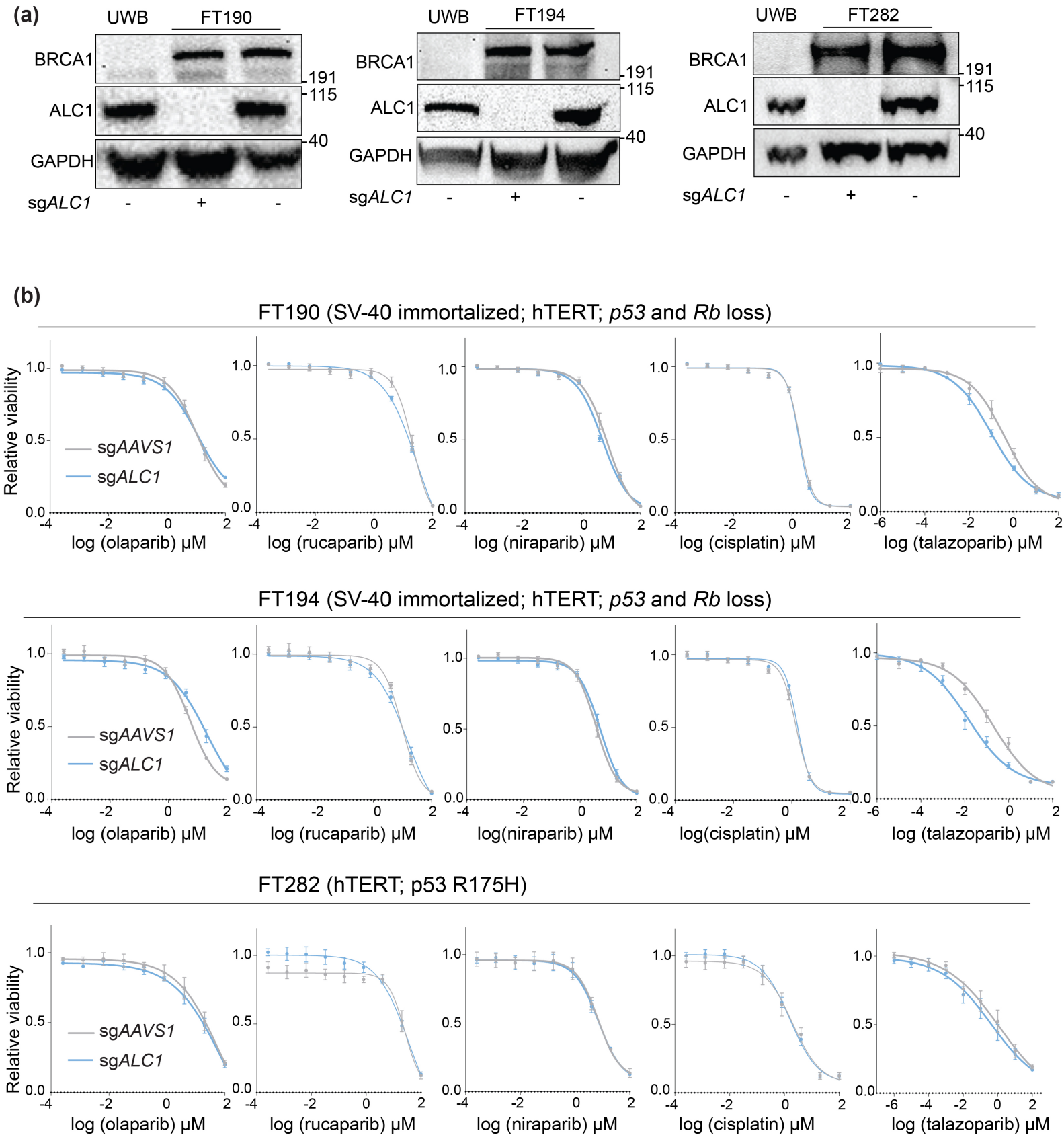
(a)
UWB
FT190
BRCA1
ALC1
GAPDH
191
115
40
sgALC1
-
+
-
UWB
FT194
BRCA1
ALC1
GAPDH
191
115
40
sgALC1
-
+
-
UWB
FT282
BRCA1
ALC1
GAPDH
191
115
40
sgALC1
-
+
-
(b)
FT190 (SV-40 immortalized; hTERT; p53 and Rb loss)
Relative viability
sgAAVS1
sgALC1
log (olaparib) μM
log (rucaparib) μM
log (niraparib) μM
log (cisplatin) μM
log (talazoparib) μM
FT194 (SV-40 immortalized; hTERT; p53 and Rb loss)
Relative viability
sgAAVS1
sgALC1
log (olaparib) μM
log (rucaparib) μM
log(niraparib) μM
log(cisplatin) μM
log (talazoparib) μM
FT282 (hTERT; p53 R175H)
Relative viability
sgAAVS1
sgALC1
log (olaparib) μM
log (rucaparib) μM
log (niraparib) μM
log (cisplatin) μM
log (talazoparib) μM

Figure 5. ALC1 loss does not enhances PARPi or cisplatin sensitivity in *BRCA1/2*-proficient non-cancerous immortalized fallopian tube (FT) cell lines.

(a) Immunoblot showing ALC1 depletion levels in indicated cell lines.

(b) Sensitivities of the indicated fallopian tube-derived cell lines to various PARPi and Cisplatin using the CellTiter-Glo assay; n = 3 biologically independent experiments. Data are presented as mean ± s.e.m.

Figure 6

(a)

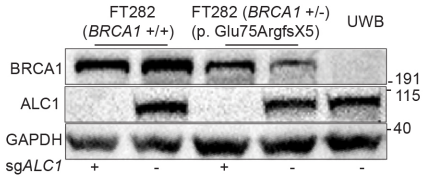

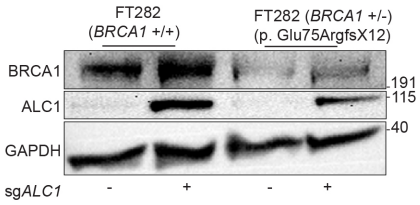

(b)

hTERT FT 282 {hTERT; p53 R175H; *BRCA1*+/c.222-223insA;(p.Glu75ArgfsX5)}_(*BRCA1* het clone 1)

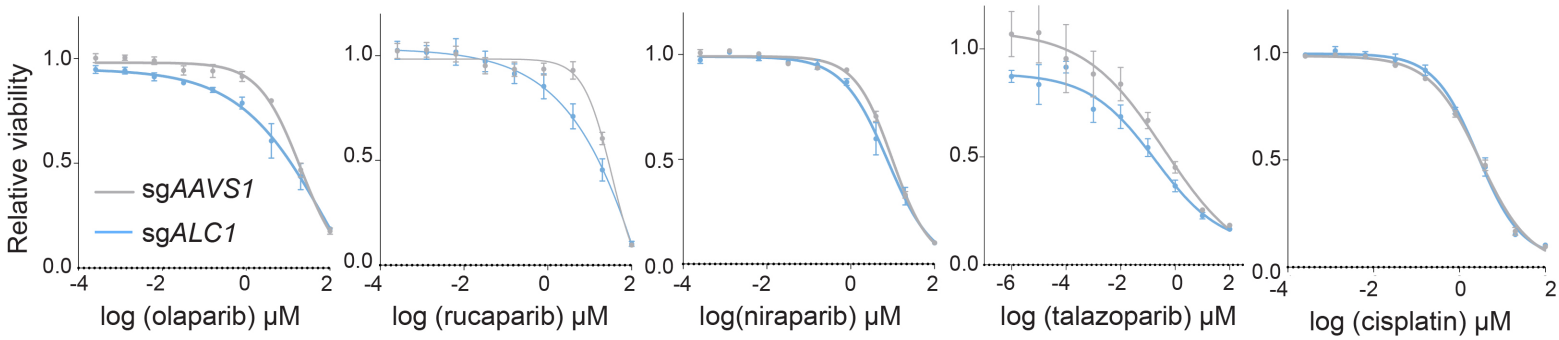

hTERT FT 282 {hTERT; p53 R175H; *BRCA1*+/c.223-226delAAAG;(p.Glu75ValfsX12)}_(*BRCA1* het clone 2)

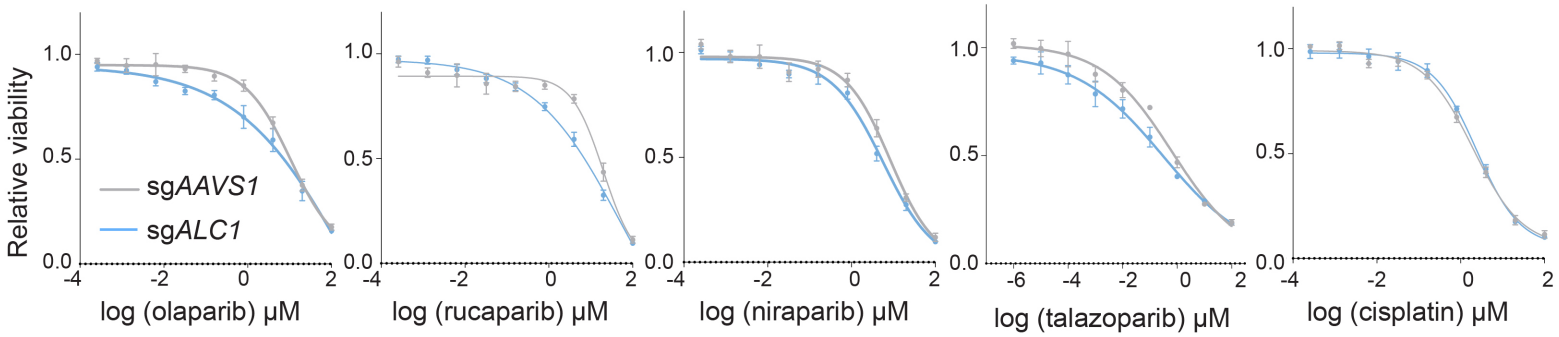

(c)

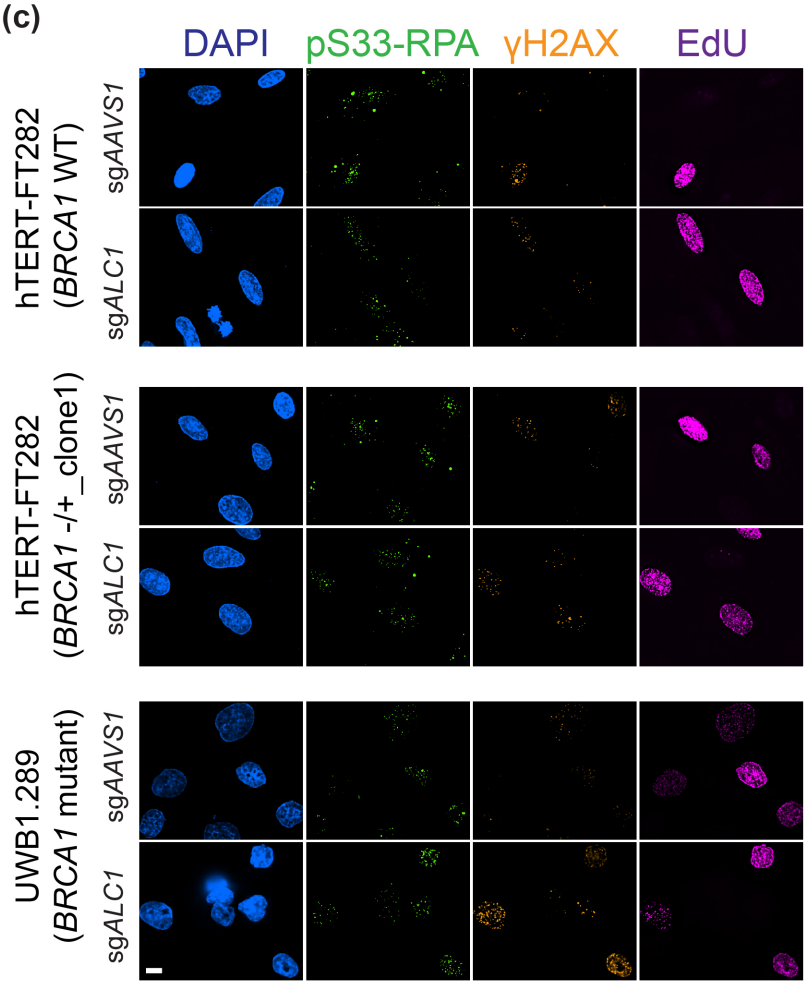

(d)

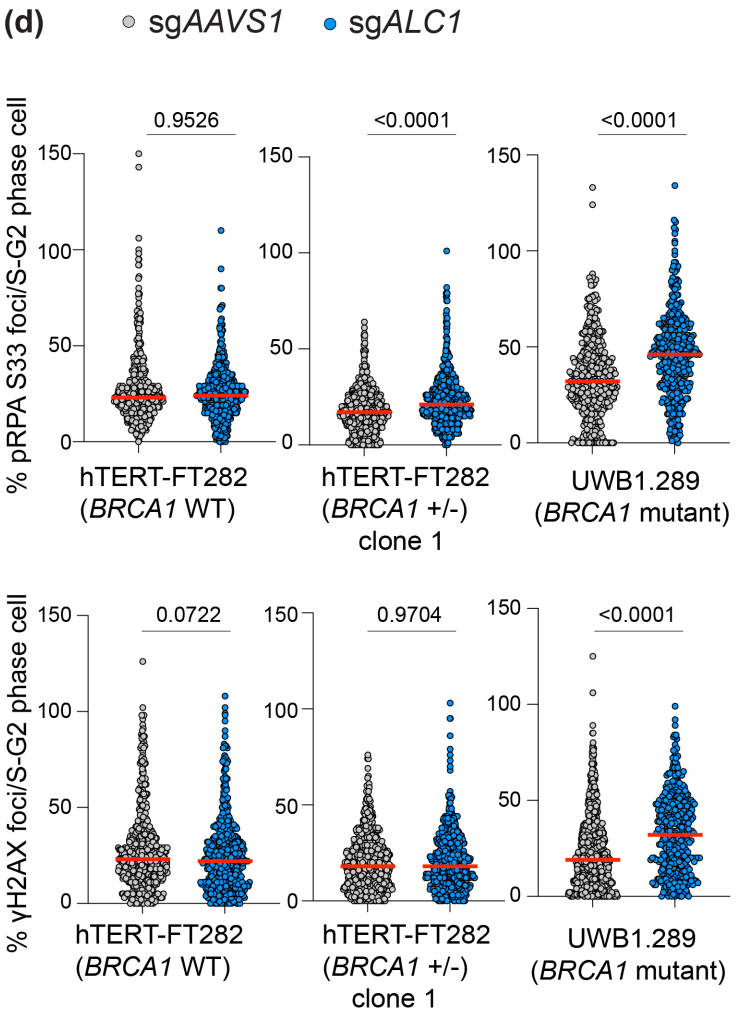

Figure 6. Loss of ALC1 does not enhance PARPi sensitivity or genome instability in *BRCA1*-heterozygous fallopian tube cell line.

(a) Immunoblot showing ALC1 depletion levels in indicated fallopian tube-derived *BRCA1*-het clones.

(b) Sensitivities of the fallopian tube-derived *BRCA1*-het clones to various PARPi and Cisplatin using the CellTiter-Glo assay; n = 3 biologically independent experiments. Data are presented as mean ± s.e.m.

(c) Representative images of pS33-RPA and γH2AX in indicated cell lines. Brightness and contrast of the images are constant between sg*AAVS1* and sg*ALC1* pair of a given cell line but are different between different cell types. Scale bar 10 micron. EdU: 5-Ethynyl-2-deoxyuridine.

(d) Quantification of pS33-RPA (top) and γH2AX (bottom) foci per S/G2 cells. n= 3 biologically independent experiments. Median is indicated in red. P-value: Mann Whitney.

Figure 7

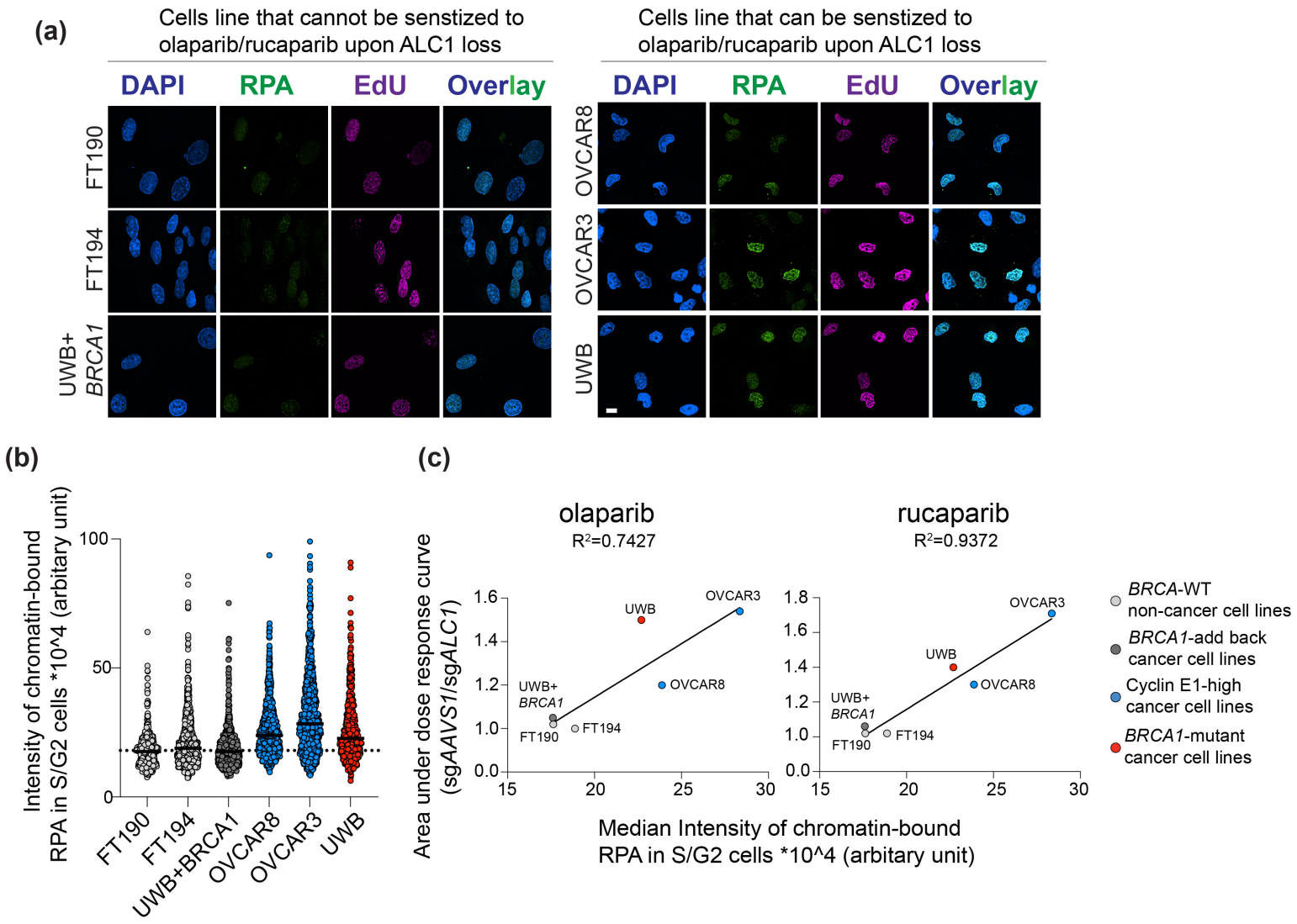
(a)
Cells line that cannot be senstized to olaparib/rucaparib upon ALC1 loss
Cells line that can be senstized to olaparib/rucaparib upon ALC1 loss
DAPI
RPA
EdU
Overlay
FT190
FT194
UWB+ BRCA1
OVCAR8
OVCAR3
UWB
(b)
Intensity of chromatin-bound RPA in S/G2 cells *10^4 (arbitary unit)
100
50
0
FT190
FT194
UWB+BRCA1
OVCAR8
OVCAR3
UWB
(c)
olaparib
R²=0.7427
rucaparib
R²=0.9372
Area under dose response curve (sgAAVS1/sgALC1)
Median Intensity of chromatin-bound RPA in S/G2 cells *10^4 (arbitary unit)
BRCA-WT non-cancer cell lines
BRCA1-add back cancer cell lines
Cyclin E1-high cancer cell lines
BRCA1-mutant cancer cell lines

Figure 7. Endogenous chromatin-bound RPA level is a critical determinant of increased PARPi sensitivity upon ALC1 loss.

(a) Representative images showing levels of chromatin-bound RPA in cells that cannot (left) or can (right) be sensitized to olaparib or rucaparib upon ALC1 loss.

(b) Quantification of chromatin-bound RPA levels in S/G2 cells in indicated cell lines. Median is indicated.

(c) Co-relation analysis between fold-enhancement in olaparib (left) and rucaparib (right) sensitivity upon ALC1 loss and chromatin-bound RPA in S/G2 cells.

Supp. Figure 1

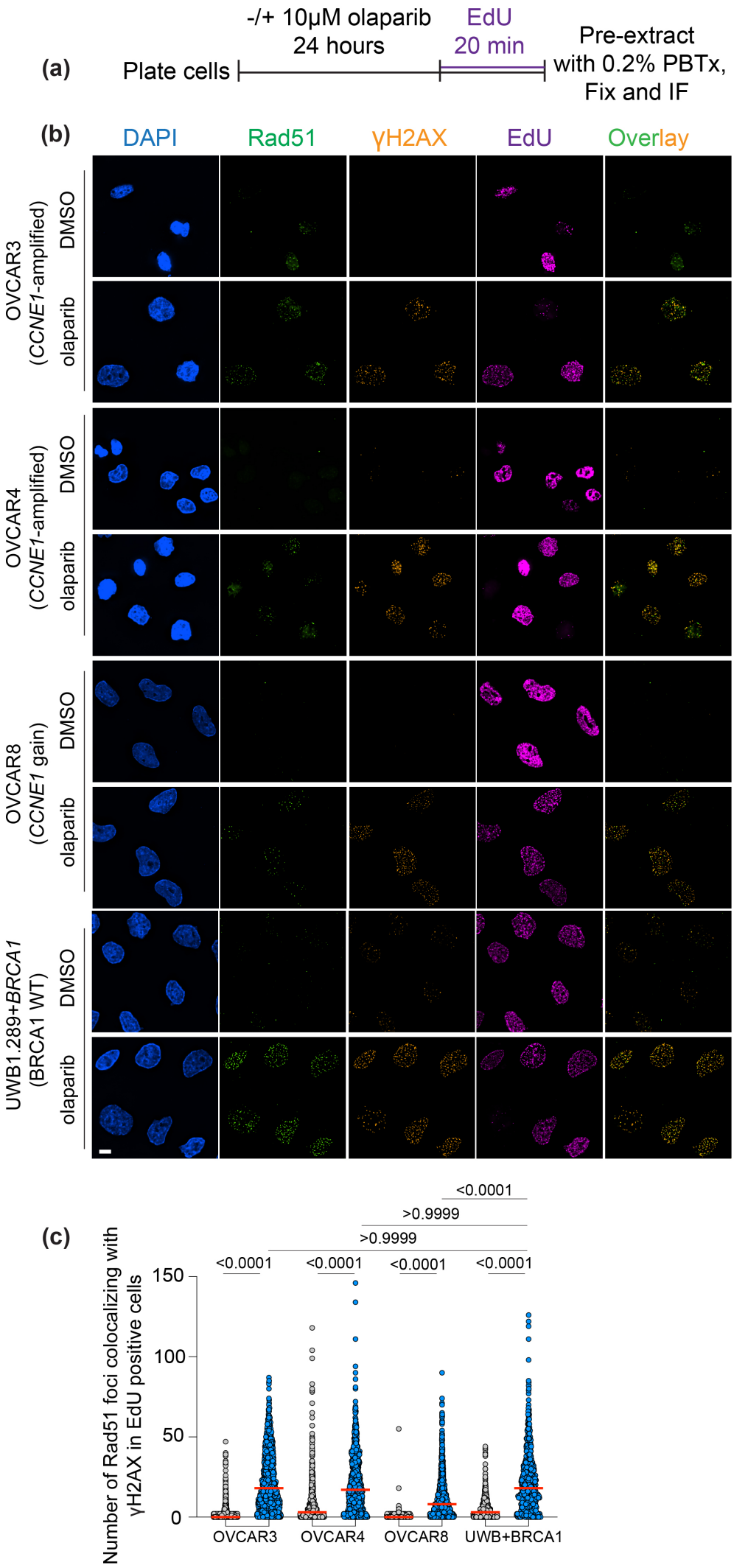

Supplementary Figure 1. Cyclin E1-high ovarian cancer cells are proficient in loading Rad51 at DNA breaks post olaparib treatment.

(a) Schematic of the experimental strategy to assess Rad51 loading post olaparib treatment.

(b) Representative images showing Rad51-γH2aX co-localized foci in indicated cell lines. Scale bar 10 microns.

(c) Quantification of Rad51-γH2AX colocalized foci in EdU positive cells of indicated cell line. Data are n=3; Median indicated. P-value: Kruskal-Wallis test.

Supp. Figure 2

(a)

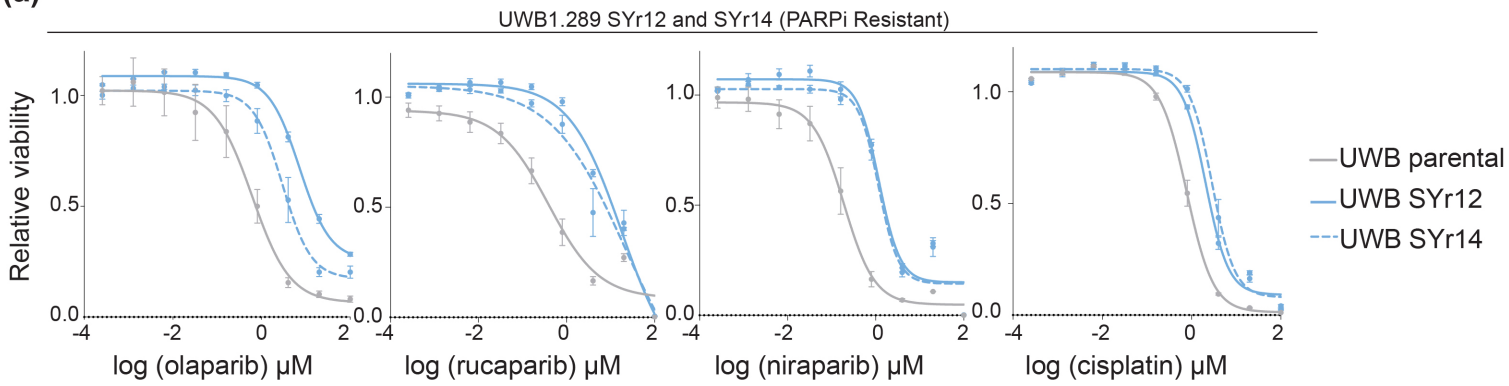

(b)

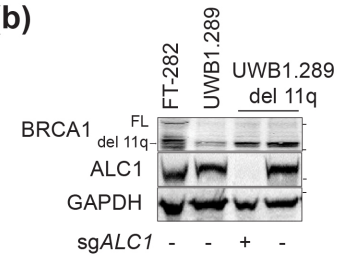

(c)

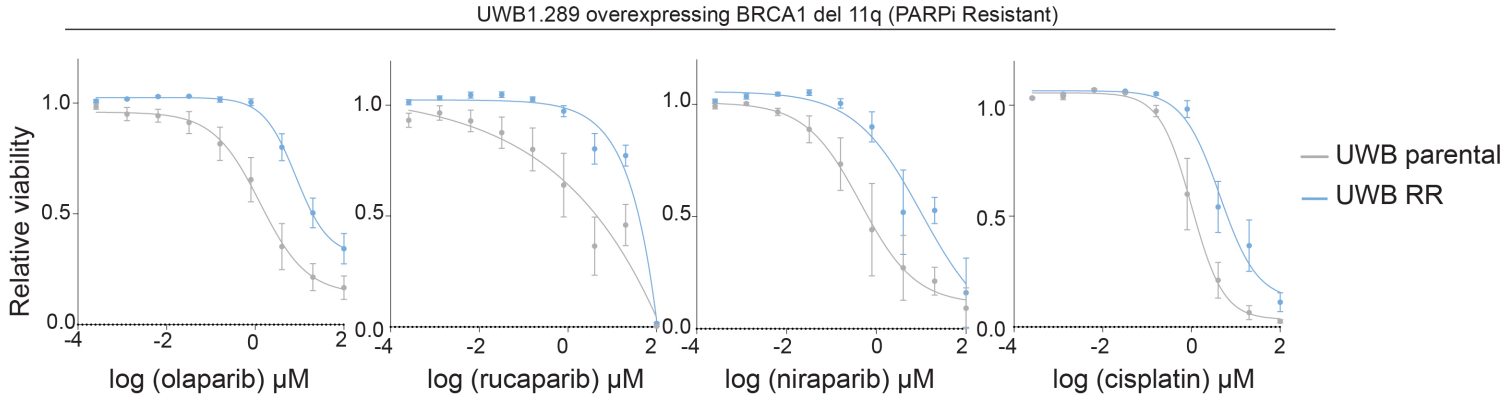

(d)

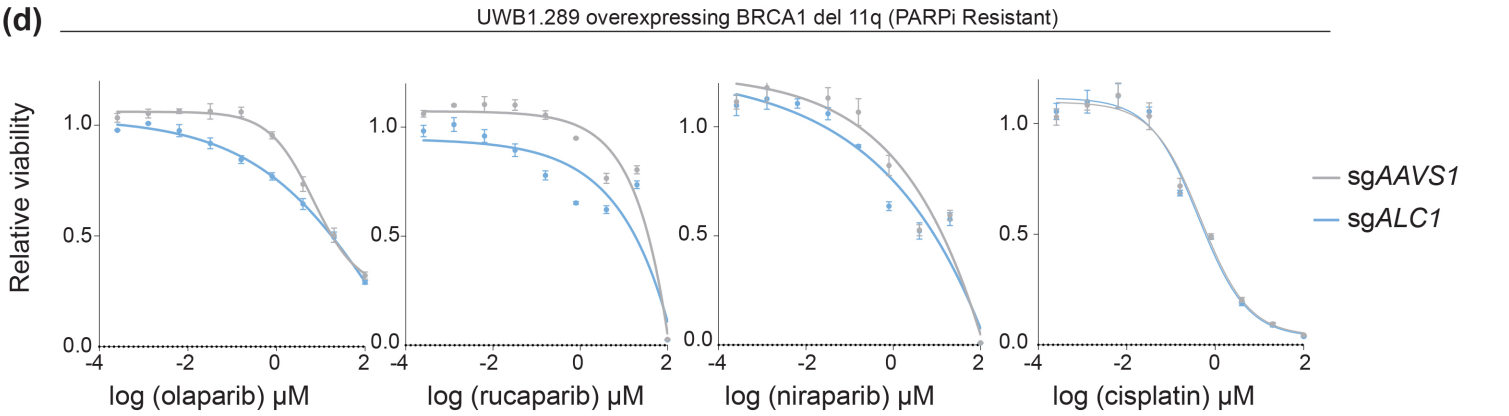

Supplementary Figure 2. ALC1 loss can enhanced PARPi sensitivity in UWB1.289 ovarian cancer cells with partially restored homologous recombination.

(a) PARPi and platinum sensitivities of the indicated UWB cell lines using the CellTiter-Glo assay; n = 3 biologically independent experiments. Data are presented as mean ± s.e.m.

(b) Immunoblot showing BRCA1 and ALC1 levels in indicated cell lines.

(c) PARPi and platinum sensitivities of the UWB-cell line overexpressing del 11q using the CellTiter-Glo assay; n = 3 biologically independent experiments. Data are presented as mean ± s.e.m.

(d) PARPi and platinum sensitivities of the del 11q overexpressing UWB cell line upon ALC1 depletion using the CellTiter-Glo assay; n = 3 biologically independent experiments. Data are presented as mean ± s.e.m.

Supp. Figure 3

hTERT FT 282 {hTERT; p53 R175H; *BRCA1*+/c.222-223insA;(p.Glu75ArgfsX5)_(BRCA1 het clone 1)

BRCA1 WT

p.Glu75ArgfsX5

hTERT FT 282 {hTERT; p53 R175H; *BRCA1*+/c.223-226delAAAG;(p.Glu75ValfsX12)_(BRCA1 het clone 2)

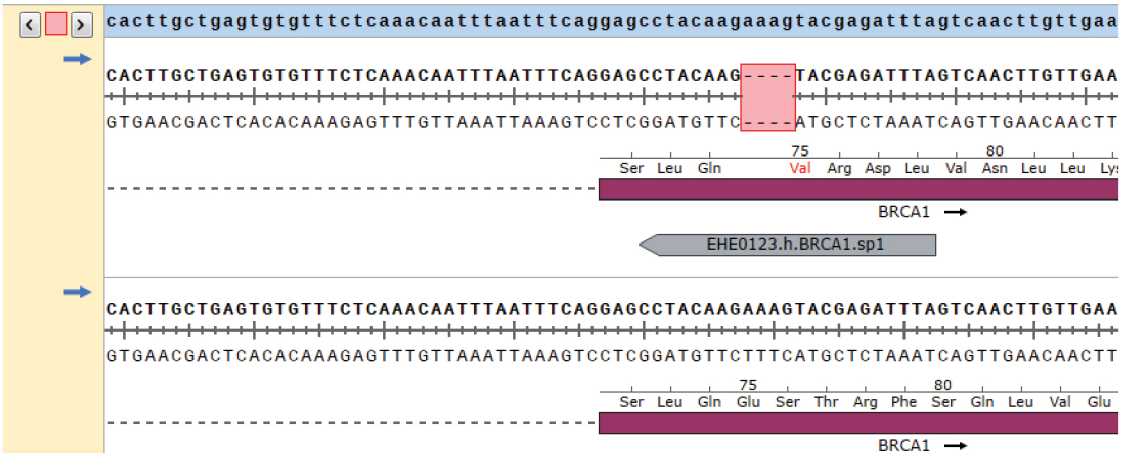

p.Glu75ValfsX12

BRCA1 WT

Supplementary Figure 3

Sequencing data showing the *BRCA1* heterozygous mutations in the two clones derived from hTERT FT282 cell line.

Case	Primary	Relapse	Autopsy
15295	0	0	7
65629	0	1	5
65862	1	0	8
65913	1	1	5
65914	1	0	3
65938	3	0	6
66114	0	0	7
66142	1	1	5
66462	2	0	7

Table 1. Number of tumor samples collected from 9 individuals on PARPi. Case number refers to the IDs in Burdett *et al*[14]. Proteomics data from this paper was analyzed to assess correlation between ALC1/CHD1L protein levels and estimated time on PARP inhibitors.

Primary Antibodies

Product	Catalog #	Lot #	Dilution used for western
Alpha-Actinin (D6F6) XP Rabbit monoclonal antibody	6487S, Cell Signaling	4	1:1000
BRCA1 (D-9) mouse monoclonal IgG2a	sc-6954, Santa Cruz	G2821	1:250
CHD1L(2170C3a) SAMPLE mouse monoclonal IgG1	sc-81065, Santa Cruz	H1721	1:1000
Anti-Cyclin E1 antibody [CCNE1/2460] mouse monoclonal IGg2b	Ab238081, Abcam	GR3437020-2	1:1000
GAPDH (14C10) rabbit monoclonal	2118S, Cell Signaling	16	1:1000
Alpha/Beta Tubulin polyclonal antibody	2148S, Cell Signaling	8	1:1000

Secondary Antibodies

Product	Catalog #	Lot#	Dilution
ECL Anti-mouse IgG, Horseradish Peroxidase linked whole antibody (from sheep)	NA931, Cytiva	17479274	1:1000
ECL Anti-rabbit IgG, Horseradish Peroxidase linked whole antibody (from donkey)	NA934, Cytiva	17348043	1:1000

Table 2: Details of antibodies used for immunoblotting